

APPENDIX F

A Numerical Investigation of the Bering Sea
Circulation Using a Linear Homogeneous Model

by

Y. J. Han* and J. A. Galt

(Contribution No. 375 from the NOAA/ERL
Pacific Marine Environmental Laboratory.)

September 1978

***Present affiliation: Department of Atmospheric Sciences**
Oregon State University,
Corvallis, OR 97331

TABLE OF CONTENTS

	Page
ABSTRACT	699
1. INTRODUCTION.	699
2. THE MATHEMATICAL MODEL AND BOUNDARY CONDITIONS.	702
2.1 The Model	702
2.2 Surface Wind Stress and Open Boundary Conditions	705
2.3 Numerical Procedures	708
3. RESULTS	713
4. SUMMARY AND SUGGESTIONS	716
5. REFERENCES.	718
TABLE	719
FIGURES	720

Abstract. A linear diagnostic model was constructed to simulate the Bering Sea circulation. Monthly mean wind stresses along with lateral water mass exchanges were used as model-forcing functions. The numerical solutions obtained for the case of annual mean wind stress generally agreed with an existing view about the **cyclonic** circulation of the seawater. The solutions obtained for each twelve-month period, however, revealed significant seasonal differences in both magnitudes and flow patterns. Additional controlled experiments indicated that the winter circulation regime was strongly influenced by wind stresses as well as lateral water mass exchanges, whereas the summer circulation regime was basically controlled by the latter. The model results also showed that the circulation is strongly bathymetry-dependent,

1. INTRODUCTION

There is currently a significant focus of scientific interest on the Bering Sea. This area has always been of particular concern to investigators supporting fisheries research in both the United States and Japan. More recently a large scale environmental assessment program sponsored by the Outer Continental Shelf office of the Bureau of Land Management has concentrated attention on potential oil development areas in Bristol Bay. **This study contains a number of components covering many scientific disciplines** which require supportive circulation information. Within the immediate future, planned expansion of the OCS study **will** extend the investigations to the north, including most of the eastern continental shelf area as far as **Norton Sound and through the Bering Strait**. In addition ~~to~~ these studies, a second large scale study, PROBES

(Productivity and **Resources of the Bering shelf**), is being planned, which will concentrate on the **trophic** level exchange in the incredibly rich fisheries located along the shelf **break**; this ecologically based study will also require circulation information.

Due largely to technical difficulties in **oceanographic observations**, our present knowledge of the Bering Sea circulation is fragmentary. The presently available observational data reveals **only uncertain knowledge of the surface current velocities and very little about** the deep basin circulation. Recently Arsen'ev (1967), Hughes et al. (1972) and Takenouti et al. (1972) compiled rather extensive field data, and **proposed** a number of alternative current schemes. Although they all shared an existing view about the **cyclonic** circulation of the sea waters, they disagreed in all the other respects: the number, location, size and even the direction of rotation of *gyres* depicted.

In the present study we attempted to explore **fundamental** physical processes of the sea using an oceanic general circulation model. A number of oceanic general circulation models have already been developed and have successfully simulated many of the observed large-scale features of the ocean currents. We have begun our study by adopting one such model (Semtner, 1974) in a simplified form.

Gurikova et al., (1964) carried out a numerical study of the Bering Sea circulation using a **linear** diagnostic model. They assumed a **flat-bottomed, laterally** closed basin, and thus investigated **only a wide-driven circulation**. The model results, however, confirmed the presence of a **cyclonic** circulation of **the** sea waters.

Lately Bacon (1973) applied the barotropic model of Galt (1973) to the Bering Sea, and examined a typical seasonal response of the western deep basin circulation. He was also able to identify, by making a series of controlled experiments, some of the important effects such as wind stress, lateral boundary forcing, and bathymetry.

The Bering Sea studies above are essentially two-dimensional and do not take into account the thermohaline component of the circulation. It would seem that any serious attempt to simulate a realistic circulation must eventually include the thermohaline effect. Accordingly, our main effort has been to model the Bering Sea in a three-dimensional way. This study is still in progress and will soon be published in part II of this series of technical reports. Meanwhile we have constructed and tested a two-dimensional diagnostic model as an initial step toward the three-dimensional modeling efforts. We have applied this simple model to the Bering Sea; this report reviews the model and its results. Section 2 contains a brief discussion of the mathematical model and the numerical procedure, together with the model boundary conditions. The results and their implications are discussed in sections 3 and 4.

2. THE MATHEMATICAL MODEL AND BOUNDARY CONDITIONS

2.1 The Model

The equations of motion for horizontal non-accelerated flow with a constant vertical eddy coefficient are:

$$-f v \rho_0 = - \frac{1}{a} \frac{\partial p}{\partial \lambda} + \rho_0 \kappa \frac{\partial^2 u}{\partial z^2} \quad (1)$$

$$f u \rho_0 = - \frac{1}{a} \frac{\partial p}{\partial \phi} + \rho_0 \kappa \frac{\partial^2 v}{\partial z^2} \quad (2)$$

The hydrostatic equation and the mass continuity equations are:

$$\frac{\partial p}{\partial z} = - g \rho_0 \quad (3)$$

$$\frac{1}{a \cos \phi} \frac{\partial u}{\partial \lambda} + \frac{1}{a \cos \phi} \frac{\partial}{\partial \phi} (v \cos \phi) + \frac{\partial w}{\partial z} = 0 \quad (4)$$

In these equations spherical coordinates are used, with λ , ϕ , and z representing longitude, latitude, and height. The fluid is contained between the surface $z = \eta$ and the bottom $z = -H(\lambda, \phi)$. The model specifies two horizontal velocities and pressure. The model assumes the fluid is homogeneous; thus the density ρ_0 is a constant ($\rho = 1$).

The boundary conditions are:

$$\kappa \rho_0 \frac{\partial u}{\partial z} = \tau_0^\lambda; \quad \kappa \rho_0 \frac{\partial v}{\partial z} = \tau_0^\phi \quad \text{and} \quad w = \left(\frac{u}{a \cos \phi} \frac{\partial \eta}{\partial \lambda} + \frac{v}{a} \frac{\partial \eta}{\partial \phi} \right) \quad \text{at } z = \eta \quad (5)$$

$$\kappa \rho_0 \frac{\partial u}{\partial z} = \tau_b^\lambda; \quad \kappa \rho_0 \frac{\partial v}{\partial z} = \tau_b^\phi \quad \text{and} \quad w = - \left(\frac{u}{a \cos \phi} \frac{\partial H}{\partial \lambda} + \frac{v}{a} \frac{\partial H}{\partial \phi} \right) \quad \text{at } z = -H(\lambda, \phi) \quad (6)$$

In equations (5) and (6) η is the free surface elevation; H is the depth of the sea; and $\tau_b^\lambda, \tau_b^\phi$ are the bottom stress components. Assuming that $\eta/H \ll 1$, we impose the boundary condition (5) at $z = 0$.

Then the momentum equations (1) and (2) are vertically averaged to yield:

$$-f\bar{v} = -\frac{\rho_0 g}{a \cos\phi} \frac{\partial \eta}{\partial \lambda} + \frac{1}{H} (\tau_o^\lambda - R\bar{u}), \quad (7)$$

$$f\bar{u} = -\frac{\rho_0 g}{a} \frac{\partial \eta}{\partial \lambda} + \frac{1}{H} (\tau_o^\phi - R\bar{v}) \quad (8)$$

where

$$\bar{u} = \frac{1}{H} \int_{-H}^0 u dz \quad (9)$$

$$\bar{v} = \frac{1}{H} \int_{-H}^0 v dz \quad (10)$$

In equations (7) and (8) the component bottom stresses are taken as $R\bar{u}$ and $R\bar{v}$ where R is the coefficient of friction ($R = 0.02$ m/s). Integration of the continuity equation (4) with boundary conditions (5) and (6) yields:

$$\frac{1}{a \cos\phi} \frac{\partial}{\partial \lambda} \left(\int_{-H}^0 u dz \right) + \frac{1}{a \cos\phi} \frac{\partial}{\partial \phi} \left(\int_{-H}^0 v dz \right) = 0 \quad (11)$$

Equation (11) simply states that the vertically integrated flow is horizontally nondivergent, which guarantees the existence of a transport stream function ψ such that

$$\bar{u} = \frac{1}{H} \int_{-H}^0 \rho_0 u dz = -\frac{1}{a} \frac{1}{H} \frac{\partial \psi}{\partial \phi} \quad (12)$$

$$\bar{v} = \frac{1}{H} \int_{-H}^0 \rho_0 v dz = \frac{1}{H} \frac{1}{a \cos \phi} \frac{\partial \psi}{\partial \lambda} \quad (13)$$

Substituting equations (12) and (13) into (7) and (8), and applying the cur_z^1 operator, defined by

$$\text{cur}_z^1 (q_1, q_2) = \frac{1}{a \cos \phi} \left[\frac{\partial p_2}{\partial \lambda} - \frac{\partial}{\partial \phi} (q_1 \cos \phi) \right] \quad (14)$$

and simplifying by eliminating a factor of $1/(a^2 \cos \phi)$, we get:

$$\begin{aligned} R \left[\frac{\partial}{\partial \lambda} \left(\frac{1}{H \cos \phi} \frac{\partial \psi}{\partial \lambda} \right) + \frac{\partial}{\partial \phi} \left(\frac{\cos \phi}{H^2} \frac{\partial \psi}{\partial \phi} \right) \right] + \frac{\partial}{\partial \phi} \left(\frac{f}{H} \right) \frac{\partial \psi}{\partial \lambda} - \frac{\partial}{\partial \lambda} \left(\frac{f}{H} \right) \frac{\partial \psi}{\partial \phi} \\ = \frac{\partial}{\partial \lambda} \left(\frac{a \tau_0^\phi}{H} \right) - \frac{\partial}{\partial \phi} \left(\frac{a \cos \phi}{H} \tau_0^\lambda \right) \end{aligned} \quad (15)$$

Equation (15) is an **inhomogeneous**, linear, elliptic, second-order partial differential equation for the **stream** function ψ . For a given bathymetry $H(\lambda, \phi)$ and a prescribed surface stress **distribution** $\tau_0^\lambda(\lambda, \phi)$ and $\tau_0^\phi(\lambda, \phi)$, the stream function ψ can be reobtained by inverting the second order differential operator. It is necessary to specify boundary **conditions** for this inversion. If the domain is **singly** connected, an **arbitrary** value can be specified as the value of the stream function on the boundary in general. However, the domain of ψ will be a multiple connected region whose boundary consists of a primary continent and several islands.

On the chosen **continent**, ψ can be held constant, but on the islands ψ must be obtained as a part of the total solution. In order to obtain the ψ on the islands, we use the method of "hole relaxation" by **Takano** (1974). Since the surface elevation η is a single valued function, a line integral of $\nabla \eta$ around the coast line of each island should vanish. By applying this condition in integrating equations (7) and (8) around each island, the following equation is obtained to predict **the ψ** on the island:

$$\oint \frac{1}{H} \left(\tau_o^\lambda + \frac{R}{aH} \frac{\partial \psi}{\partial \phi} \right) a \cos \phi \, d\lambda + \oint \frac{1}{H} \left(\tau_o^\phi - \frac{R}{H a \cos \phi} \frac{\partial \psi}{\partial \lambda} \right) a \, d\phi = 0 \quad (16)$$

In the above, the fact that ψ is spatially constant along the coastline eliminates any contribution from the **Coriolis** terms.

We solve equations (15) and (16) simultaneously by the "successive over-relaxation method." It should be mentioned, however, that the highest order terms in equation (15) involve a small friction parameter R , and thus special care must be taken to maintain stability of the numerical methods. This plus the numerical procedure for solving Equation (15) and (16) will be discussed in section 2.3.

2.2 Surface Wind Stress and Open **Boundary** Conditions

Wind stress can be estimated by conventional drag law methods if the surface wind is known. Unfortunately, wind measurements over the Bering Sea are very sparse in space and **time**, since they generally come from a handful of ship stations. Therefore, for the numerical models,

wind stress is computed from surface pressure data. First, monthly mean pressure data provided by the National Climate Center were interpolated quadratically from a $5^\circ \times 5^\circ$ grid mesh onto the model grid mesh of 2° (long.) \times 1° (lat.). The interpolated pressure data were then used to estimate the **geostrophic** wind velocity, and the wind velocity at anemometer height was obtained by multiplying the **geostrophic** wind speed by a factor γ and changing the **geostrophic** wind direction by angle α (the constant γ is .07; α is 190). Strictly speaking, one should use synoptic maps in estimating wind stress because the variable part of the pressure could increase the wind stress estimate through the non-linearity of the drag law. In fact, the studies by Aagaard (1970) and Fissel et al. (1977) strongly suggest that the stress computed from the monthly mean pressure could be easily underestimated by a factor of 2 or 3. On the basis of this study, we multiplied the monthly mean stress by 3.0 for the model calculation.

The annual mean wind stress was computed by averaging 12 months of wind stress data. This is shown in **Figure 1**. The computed monthly mean wind stress patterns for January through December are shown in Figures 2-13. The January map shows a typical winter pattern characterized by the northeasterly stress associated with a strong high pressure center over Siberia and low pressure center over the North Pacific Ocean. The stress pattern in August, on the other hand, shows a very weak stress over most of the sea and somewhat stronger "southwesterly stress over the southeast part of the basin. In general, the wind forcing in summer

is weaker by one order of magnitude than in winter. This significantly large winter-to-summer change in the wind stress might lead to large annual signals in the resulting currents. Recent work by Kinder, et al. (1975) has suggested that variations in the wind stress may result in planetary wave patterns that control the current structure along the Bering Sea **shelf** break. Although the present model does not include any such wave dynamics in its steady state formulations, the time-dependent problem is of considerable theoretical interest. For this reason the complete annual cycle by months has been included. To the authors' knowledge the analysis of these monthly mean pressure data to yield sequential stress patterns is not available elsewhere; We hope that this effort will help stimulate productive consideration of the more complete time-dependent problem. **In** addition to stress fields, the model requires boundary conditions.

At the open boundaries of the grid, estimates of vertically integrated transports were required. The model has four open boundaries along the Aleutian - Commander Island Arc: **Kamchatka** Strait, Commander - Near Strait, Central Aleutian Pass and Western Aleutian Pass. The Bering Strait also **modelled** as an open boundary. The widths and depths of the open boundaries are adjusted to match the observed **bathymetry** within the limits imposed by grid resolutions. Integrated volume transport values on the open sections are chosen from various estimates presently available. It should be mentioned, however, that at the present stage there are many uncertainties in transport estimates at the various passes.

The chosen values of (annual mean) transports are given in Table 1. A net transport of 18 sv (1 sv = $10^6 \text{ m}^3/\text{s}$.) outward through the Kamchatka Strait is in close agreement with an estimate of 18.4 sv by Arsen'ev (1967) and summer values (20sv) by Hughes et al. (1974). A net transport of 14sv inward across the Commander - Near Strait, taken from Arsen'ev (1967), is greater than an estimate (10SV) by Favorite (1974) but less than Hughes et al. (25sv). The total inflows through the Western and Central Aleutian are based on the estimates made by Arsen'ev (1967). For the Bering Strait, the total transport (1sv) outward was chosen from the estimate (1.1sv) by Arsen'ev (1967).

2.3 Numerical Procedures

The basic equations (15) and (16) for the volume flux stream function ψ are solved numerically by finite-difference methods. The Bering Sea domain is approximated by a collection of rectangles, each having horizontal dimensions corresponding to increments $\Delta\lambda$ and $\Delta\phi$ in longitude and latitude. The boundary grid is chosen so as to best approximate the coastline (Fig. 14).

We write the basic equation (15) in a compact form using Cartesian coordinates:

$$R \nabla^2 \psi + A \frac{\partial \psi}{\partial x} + B \frac{\partial \psi}{\partial y} = \phi . \quad (17)$$

where A, B and ϕ are functions of bottom slope, planetary vorticity gradient and the wind stress distribution.

Let the nodes (Fig. 15) be labeled $x = i, x + d = i + 1, x - d =$

$i - 1, y = j, y + d = j + 1, y - d = j - 1$. Then at the nodes (i, j) ,

Equation (17) has the finite difference form:

$$R \left[\frac{1}{d^2} (\psi_{i+1, j} + \psi_{i, j+1} + \psi_{i-1, j} + \psi_{i, j-1} - 4\psi_{i, j}) \right] + \frac{A}{2d} (\psi_{i+1, j} - \psi_{i-1, j}) + \frac{B}{2d} (\psi_{i, j+1} - \psi_{i, j-1}) = \phi_{i, j} \quad (18)$$

Solving for $\psi_{i, j}$ leads to

$$4\frac{R}{d^2} \psi_{i, j} = \left(\frac{R}{d^2} + \frac{A}{2d}\right) \psi_{i+1, j} + \left(\frac{R}{d^2} + \frac{B}{2d}\right) \psi_{i, j+1} + \left(\frac{R}{d^2} - \frac{A}{2d}\right) \psi_{i-1, j} + \left(\frac{R}{d^2} - \frac{B}{2d}\right) \psi_{i, j-1} - \phi_{i, j} \quad (19)$$

Thus ψ is defined at each grid point in terms of ψ at four neighboring grid points, each weighted by a factor related to the grid size, depth, bottom slope and wind stress.

Approximating the differential equation (17) by the finite difference equation (19), we obtain a system of linear algebraic equations. One efficient method of solving this type of equation is that of "successive over-relaxation." For solution convergence, however, the matrix of equation (19) must be diagonally dominant, i.e., the sum of the off diagonal elements in any row of the coefficient matrix must be less than or equal to the diagonal element in that row. The condition to be met here is:

$$\left| \frac{R}{d^2} + \frac{A}{2d} \right| + \left| \frac{R}{d^2} + \frac{B}{2d} \right| + \left| \frac{R}{d^2} - \frac{A}{2d} \right| + \left| \frac{R}{d^2} - \frac{B}{2d} \right| \leq 4 \frac{R}{d^2} \quad (20)$$

This condition will be met if:

$$|A| \leq \frac{2R}{d}, \quad (21)$$

$$|B| < \frac{2R}{d}. \quad (22)$$

Thus, three factors are critical in obtaining a converging solution: **bottom slope, friction coefficient and grid size. Clearly conditions (21) and (22) can always be satisfied by making d small enough. In practice, however, the number of iterations and the storage requirements increase as d decreases.**

Sarkisian (1976) recognized this difficulty and proposed an alternative; the "method of directional differences." We used this method for the present study. The essence of the method is quite simple: Depending on the sign of the coefficients, forward or backward finite differences are used for the first-order derivatives in such a way that diagonal terms possess the maximum weights. For instance, in Equation (17), following **Sarkisian's** notation, we substitute the derivative with respect to x by the directional difference relation in the following way:

$$d\left(\frac{\partial \psi}{\partial x}\right) = \delta_1 \psi_{i+1,j} + (1-2\delta_1) \psi_{i,j} + (\delta_1-1) \psi_{i-1,j} \quad (23)$$

where $\delta_1 = 0$ for $A_{i,j} < 0$

$\delta_1 = 1$ for $A_{i,j} > 0$

Similarly,

$$d\left(\frac{\partial \psi}{\partial y}\right) = \delta_2 \psi_{i,j+1} + (1-2\delta_2) \psi_{i,j} + (\delta_2-1) \psi_{i,j-1} \quad (24)$$

where $\delta_2 = 0$ for $B_{i,j} < 0$

$\delta_2 = 1$ for $B_{i,j} > 0$

If we write the finite-difference analogue of the sum $A \frac{\partial \psi}{\partial x} + B \frac{\partial \psi}{\partial y}$, then $\psi_{i,j}$ has the coefficient $[|A_{i,j}| + |B_{i,j}|]$ in this sum. Thus the diagonal predominance is present in the system of algebraic equations

obtained, independent of the signs of the coefficients A and B. The Laplace operator is written as in equation (18). Then we obtain the following difference approximation of equation (17):

$$\begin{aligned} & \frac{R}{d^2} [\psi_{i-1,j} + \psi_{i+1,j} + \psi_{i,j-1} + \psi_{i,j+1} - 4\psi_{i,j}] \\ & + A_{i,j} \frac{\delta_1 \psi_{i+1,j} + (1 - 2\delta_1) \psi_{i,j} + (\delta_1 - 1) \psi_{i-1,j}}{d} \\ & + B_{i,j} \frac{\delta_2 \psi_{i,j+1} + (1 - 2\delta_2) \psi_{i,j} + (\delta_2 - 1) \psi_{i,j-1}}{d} = \phi_{i,j} \quad (25) \end{aligned}$$

The computation of the stream function on islands remains to be discussed. Rather than construct a finite difference version of equation (16) directly, we use an indirect approach which is based on a finite-difference form of Stokes theorem (see Semtner (1974)). This theorem applies to any area A covered by a collection of rectangles and having a perimeter P of rectangle edges. If arbitrary values of two fields q_1 and q_2 are defined at the corners of rectangles, the following can be shown to hold:

$$\sum_A \sum \left[\frac{\partial}{\partial x} (\bar{q}_2^y) - \frac{\partial}{\partial y} (\bar{q}_1^x) \right] \Delta x \Delta y$$

$$= \sum_P (\bar{q}_1^x \Delta x + \bar{q}_2^y \Delta y) \quad (26)$$

where $\bar{q}_1^x = \frac{q_1(x) - q_1(x+d)}{2}$

$$\bar{q}_1^y = \frac{q_1(y) + q_1(y+d)}{2}$$

To compute the value of the island stream function, a **line integral** of equations (7) and (8) is **required**. The curl of those equations is already available in equation (25). **By** virtue of the Stokes theorem above, we can equivalently take the area sum of equation (25). (We can arbitrarily **set the values of stress to be zero at the interior corners of rectangles**, then the area sum will pick up non-zero at the interior corners of rectangles on the margin of the area.) The resulting area sum **gives** an algebraic relation between the value **of ψ** for an island and all the values **of ψ** immediately surrounding the island. This relation is solved simultaneously with equation (25) at each grid point in the Bering Sea domain.

3. RESULTS

Solutions were obtained first for the case of annual mean wind stress (Fig. 1) and mean mass flux conditions (Table 1) specified at the open passes. Solutions for each twelve-month period were also obtained, but due to the lack of data, monthly variations of the lateral boundary mass fluxes were not taken into account; an annual mean flux condition was used in the calculations. Additional model parameters are given in Appendix B.

With the annual mean wind stress from the general direction of north-east, contours of the stream function for the whole Bering Sea (Fig. 16) show a strong **cyclonic** gyre in the western half of the basin, and a somewhat complicated but much weaker flow (less than 2 sv.) in the eastern shelf region. More specifically, the Pacific Ocean **waters entering through** the open passes along the Aleutian Islands chain first move eastward along the Aleutians, and then turn northwestward along the **shelf** break to form a broad cross basin flow. A little south of Cape **Navarin** this cross basin current branches into two parts: the **main part flows southwest**, the second part flows toward the Bering Strait. The southwest-bound current moving parallel to Koryak Coast and **Shirshov** Ridge finally flows through the Kamchatka Strait into the Pacific Ocean.

The mass transport vectors computed from Equation (12) and Equation (13) for the annual mean case are shown in Figure 17. To show a clearer picture of the circulation pattern in the deep basin, that portion was magnified and is shown in Figure 18. The flow pattern, of course, is consistent with the stream function field described above. It must be

remembered, however, that the transport velocity vectors do not characterize the motion of the water particles but give only a picture of the overall water transport in the whole vertical column of the layer. In other words, the actual current pattern at a certain level could be substantially different from the transport pattern. Nonetheless, the results obtained are of definite importance for establishing the nature of the mean circulation of the sea.

To illustrate the monthly average characteristics of the total current, transport stream **functions** for January through December were calculated. Judging from these maps, the average, **longterm** current in the deep basin is basically **cyclonic**, which agrees with the **annual** mean case. There are, however, significant differences in both magnitudes and flow patterns between the winter regime and the summer regime.

In the winter season, the flow in the deep basin is characterized by three strong **cyclonic subgyres**. These subgyres are established in November and retained through the winter months (**November-March**) reaching a maximum strength in February (Fig. 19). The strong cross-basin transport along the shelf break is another characteristic of the winter regime. It extends from the southeast corner of the basin to the south of Cape **Navarin**. The flow in the shelf region **appears to** be quite complicated; it even shows an **anticyclonic** gyre in the Gulf of Anadyr. Unfortunately, due to a wide coverage of pack ice over the shelf in winter, there are no field data available to verify the model results. **We** might conjecture **at** most that the flow under the ice sheet probably resembles **the** model result, but this is not certain.

The transition to summer is characterized by weakening of both the **subgyres** in the deep basin and the cross-basin transport along the shelf break. The **subgyres completely disappear in May** and reappear in October. The pattern for August is seen in Figure 20. The deep basin circulation becomes weaker and tends to confine itself in the **vicinity** of the **source-sink** region as the season progresses. The seasonal differences of the flow regime in the present study must be attributed to seasonal variation of the wind stress since the model assumed a fixed mass flux boundary condition. This was further investigated in a series of controlled experiments; one with wind forcing only (fig. 21), and the other with a **source-sink** only (Fig. 22). Evidently, the summer circulation closely resembles the one with the source-sink only. This might indicate that the circulation in summer, is primarily driven by the mass source-sink specified along the boundary mainly due to the absence of strong wind. On the other hand, the closed gyres of the deep basin in winter are direct consequences of wind forcing, which showed up clearly in the experiment with wind forcing only,

4. SUMMARY AND SUGGESTIONS

The present diagnostic study attempts to establish a basis for a three-dimensional prognostic modeling of the Bering Sea. The model performances are very encouraging; a simple model such as this can be valuable for exploring some fundamental physical processes in the Bering Sea. The results obtained generally agree with the existing flow features as inferred from the **climatological** hydrographic data. Seasonal characteristics of the model flow, however, are yet to be verified with the observational data.

Furthermore, the present study provides us with invaluable information on the range of model parameters such as bottom topography, wind stress, etc. This information has already been used in our initial calibration of a three-dimensional model.

Based on the analysis of the present study, we propose a few **suggestions:**

1) A numerical model with a finer **grid** resolution is needed to handle the narrow passage along the Aleutian chain and to adequately resolve the bottom topography of the sea. There is a strong indication that the model flow depends upon the prescribed boundary mass flux conditions and upon the details of bottom topography. Doubling the present **grid resolution** (100 X 100 km) should improve the results significantly.

2) A more accurate estimate of wind stress over the Bering Sea is certainly necessary. The present study indicates a sensitivity of flow features to both the intensity and the pattern of driving stress. For

example, seasonal characteristics of the model flow are entirely due to seasonal variation of the imposed wind stresses. Reliable synoptic pressure maps are required in order to eliminate the use of stress **multipliers with mean pressure maps**. (This has been under investigation and **will** be reported elsewhere.)

The effect of seasonal variation of boundary mass flux on the sea circulation must be taken into account in future studies. The controlled experiment shows that the **summer** flow regime is very similar to that with the boundary mass forcing only, thus indicating the importance of boundary conditions in determining the summer regime. Future field work directed toward **measuring lateral boundary conditions will improve simulation of the interior flow**.

3) Finally, the two-dimensionality of the present model --probably the weakest point of the model--allows only vertically averaged mass circulations. These results, however, are difficult to verify with field data obtained at a fixed level because there is usually a rapid variation of magnitude and direction of the flow with depth in the real sea.

In order to simulate more realistic circulation in the Bering Sea, three-dimensional modeling based on complete equations is necessary.

5. REFERENCES

- Aagaard, K. 1970: Wind-driven transports in the Greenland and Norwegian Seas, Deep-Sea Res. 17, 281-291.
- Arsen'ev, V.S., 1967: Currents and Water Masses of the Bering Sea, **Izd. Nauka**, Moscow. (Transl., 1968, Nat. Mar. Fish. Serv., Northwest Fish. Center, Seattle, Wash.). 135 pp.
- Bacon, J.C., 1963: Numerical investigation of Bering Sea dynamics, **M.S. Dissertation**, Naval Postgraduate School.
- Favorite, F., 1974: **Flow** into the Bering Sea through Aleutian island passes, Oceanography of the Bering Sea, Hood, **D.W.** and **E.J.** Kelly, Ed., 3-37.
- Fissel, D., S. Pond and M. Miyake, 1977: Computation of surface fluxes from **climatological** and synoptic data, Monthly Weather Review 105, 26-36.
- Galt, J.A., 1973: A numerical investigation of Arctic Ocean dynamics, Journal of Physical Oceanography.
- Gurikova, K.F., **T.T. Vinokurova**, and **V.V. Natarov**, 1964: A model of the wind-driven currents in the Bering Sea in August 1958 and 1960. (Transl., 1968, in Soviet fisheries investigations in the Northeastern Pacific, Part 2, pp 48-77, **avail.** Nat. Tech. Inf. Serv., Springfield, VA, TT 67-51204).
- Hughes, F.W., **L.K.** Coachman and K. **Aagaard**, 1974: Circulation, transport and water exchange in the Western **Bering** Sea, Oceanography of the Bering Sea, Hood, **D.W.** and **W.J.** Kelly, Ed. 59-98.
- Kinder, T.H., **L.K.** Coachman and **J.A.** Galt (1975): The Bering Slope Current, Journal of Physical Oceanography, 5(2), pp 231-244.
- Sarkisian, A.S., 1976: The diagnostic calculations of a large-scale Oceanic circulation, The Sea, Vol. 6, Goldberg, E.D., Ed., 363-458.
- Semtner, A.J., 1974: An oceanic general circulation model with bottom topography, Numerical simulation of Weather and Climate, Technical Report No. 9, Department of Meteorology, University of California, Los Angeles, 99 pp.
- Takano, K., 1974: A general circulation model for **the world** ocean Numerical simulation of weather and climate, Technical Report No. 8 Department of Meteorology, University of **California, Los Angeles**, 47 pp.
- Takenouti, **A.Y.** and K. Ohtani, 1974: Currents and water masses in the Bering Sea: A review of Japanese work, Oceanography of the Bering Sea, Hood, **D.W.** and **E.J.** Kelly, Ed., 39-57.

Table 1.

Mass transport **at** open boundaries

Kamchatka Strait	- 18sv.*
Commander - Near Strait	+ 14sv.*
Western Aleutian Pass	+ 4SV.
Central Aleutian Pass	+ 1sv.
Bering Strait	- 1SV.

* - Outward

+ Inward

FIGURE CAPTIONS

- Figure 1. Annual **mean** wind stress (dyne/cm²) computed from 12 monthly mean wind stresses
- Figure 2. January mean wind stress computed from the monthly mean pressure map
- Figure 3. February mean wind stress computed from the monthly mean pressure map
- Figure 4. **March** mean wind stress computed from the monthly mean pressure map
- Figure 5. **April** mean wind stress computed from the monthly mean pressure map
- Figure 6. **May** mean wind stress computed from the monthly mean pressure map
- Figure 7. June mean wind stress computed from the monthly mean pressure map
- Figure 8. July mean wind stress computed from the monthly mean pressure map
- Figure 9. August mean wind stress computed from the monthly mean pressure map
- Figure 10. September mean wind stress computed from the monthly mean pressure map
- Figure 11. October mean wind stress computed from the monthly mean pressure map
- Figure 12. November mean wind stress computed from the monthly mean pressure map
- Figure 13. December mean wind stress computed from the monthly mean pressure map
- Figure 14. Bering sea configuration and the finite difference approximation of the Basin. Contours of depth are superimposed.
- Figure 15. Location of variables in the horizontal grid
- Figure 16. Annual mean mass transport stream functions. Contour intervals are 2 sv (_____) and 0.2 sv (---)
- Figure 17.** Velocity vectors which correspond to Figure 16
- Figure 18. Velocity vectors for the deep basin

FIGURE CAPTIONS (cont.)

- Figure **19.** February mean mass transport stream function
- Figure 20. Same as Figure 19 except for August
- Figure 21. Annual mean stream functions computed with the annual mean wind stress forcing only.
- Figure 22. Annual mean stream functions computed with the prescribed lateral mass source-sink **only.**

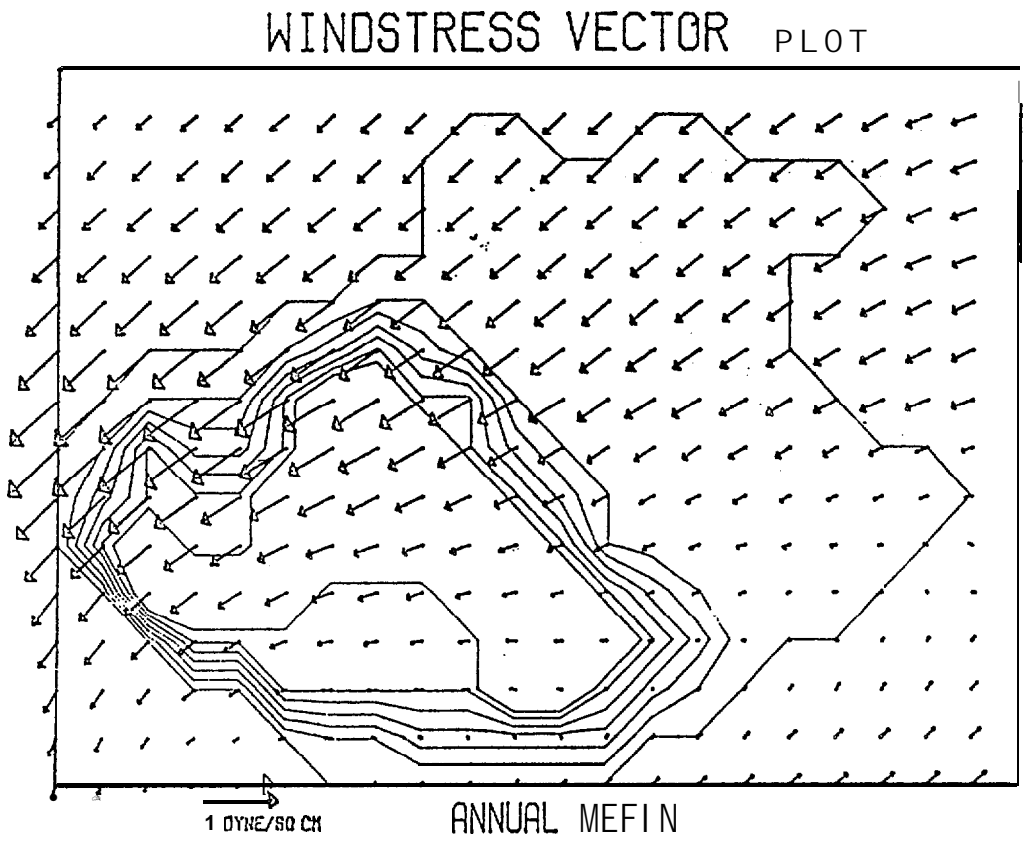


Figure 1

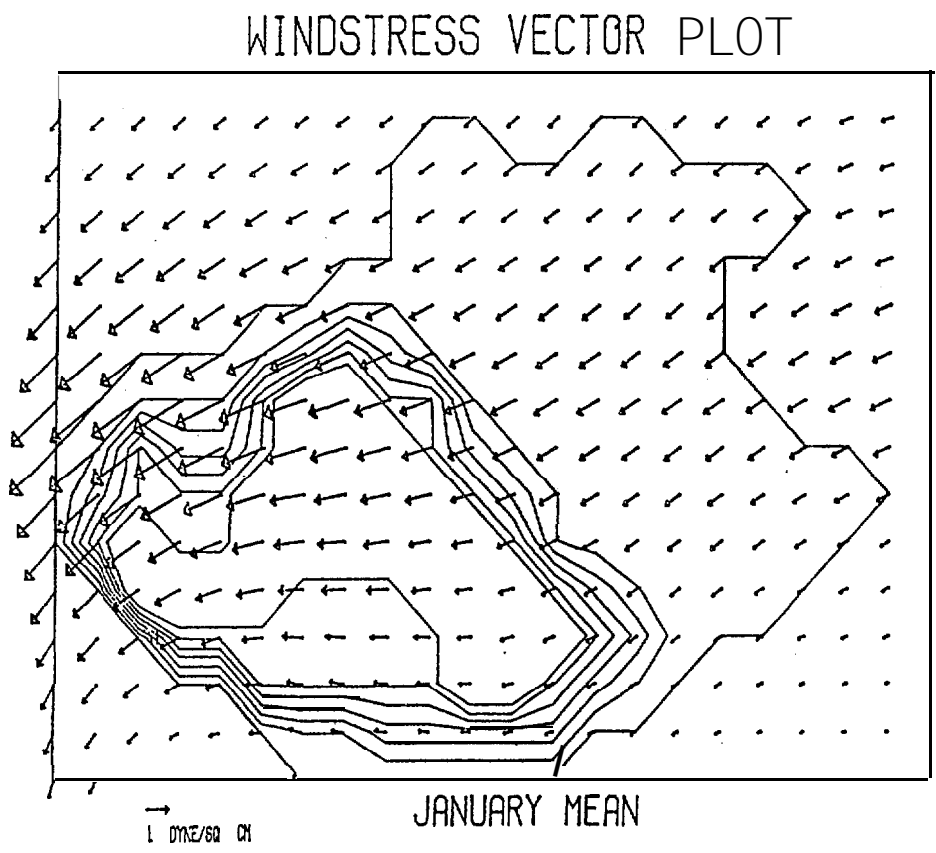
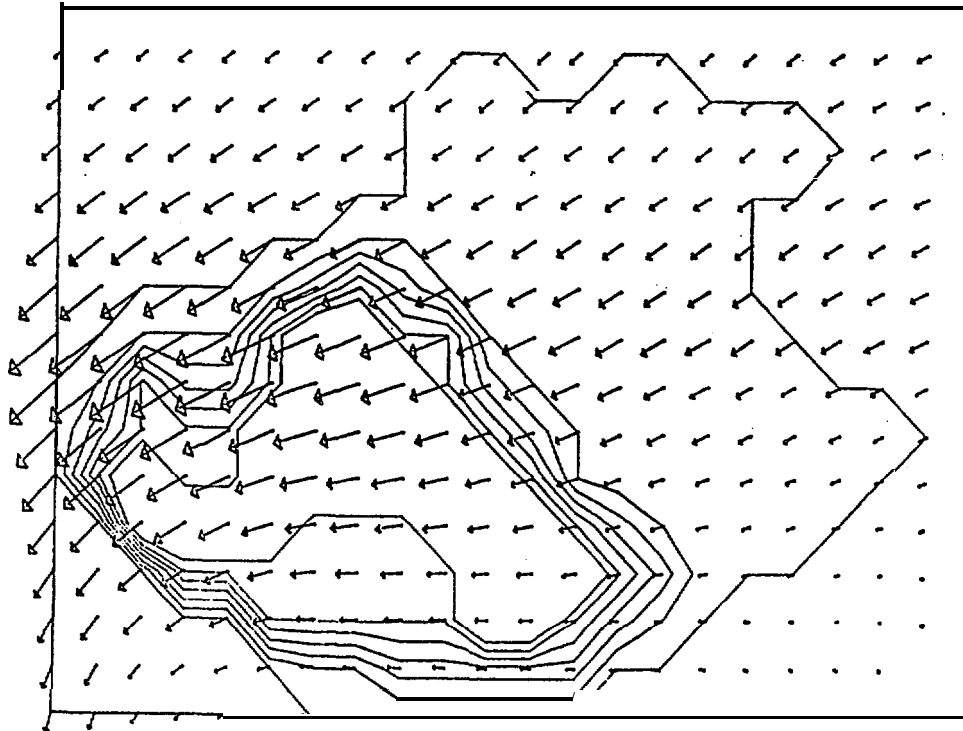


Figure 2

WINDSTRESS VECTOR PLOT

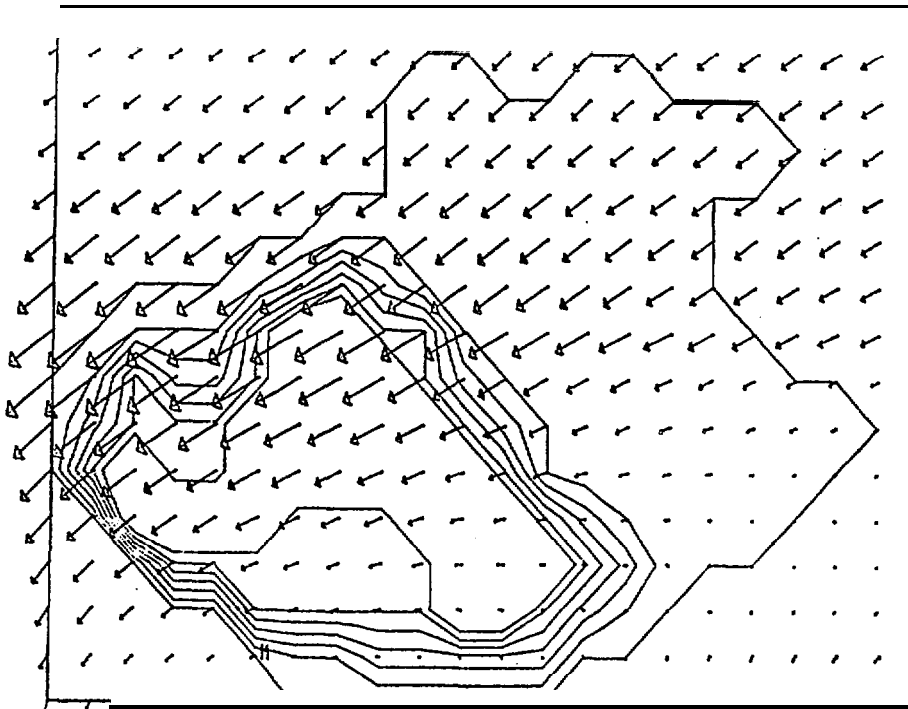


FEBRUARY MEAN

1 DYNE/SQ CM

Figure 3

WINDSTRESS VECTOR PLOT



MARCH MEAN

→
1 DYNE/SQ CM

Figure 4

WINDSTRESS VECTOR PLOT

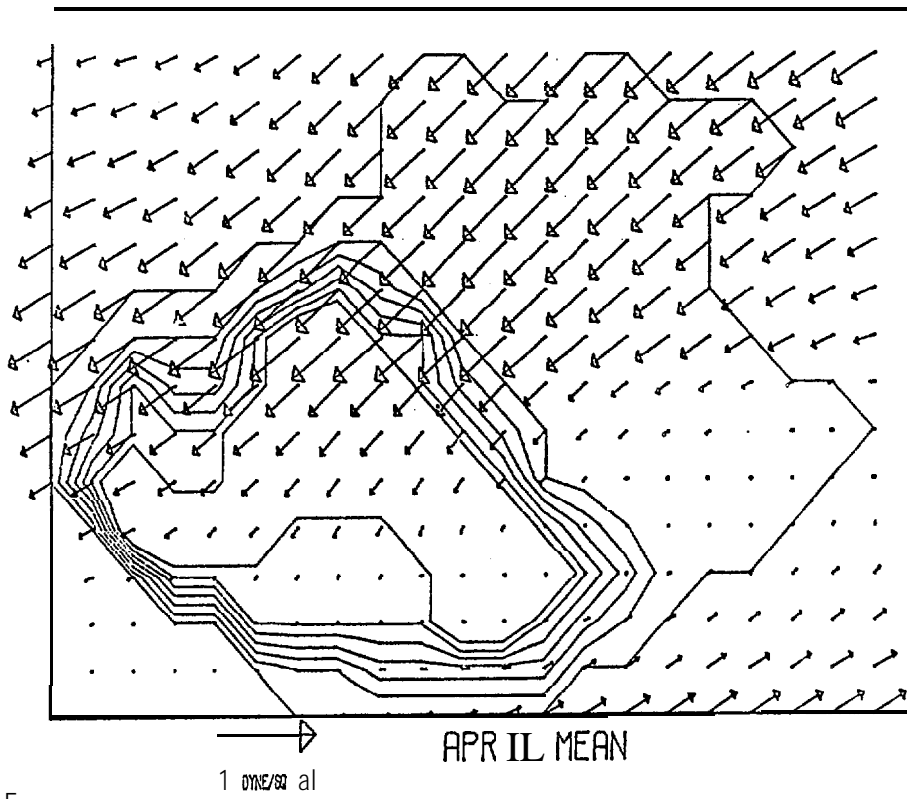


Figure 5

WINDSTRESS VECTOR PLOT

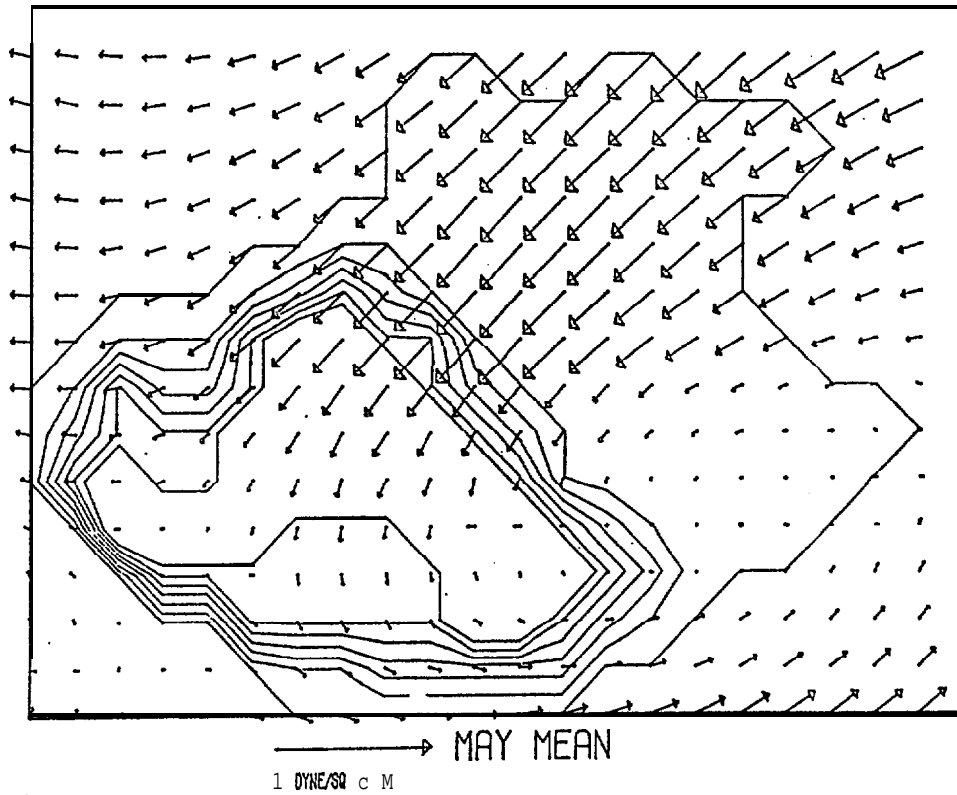


Figure 6

WINDSTRESS VECTOR PLOT

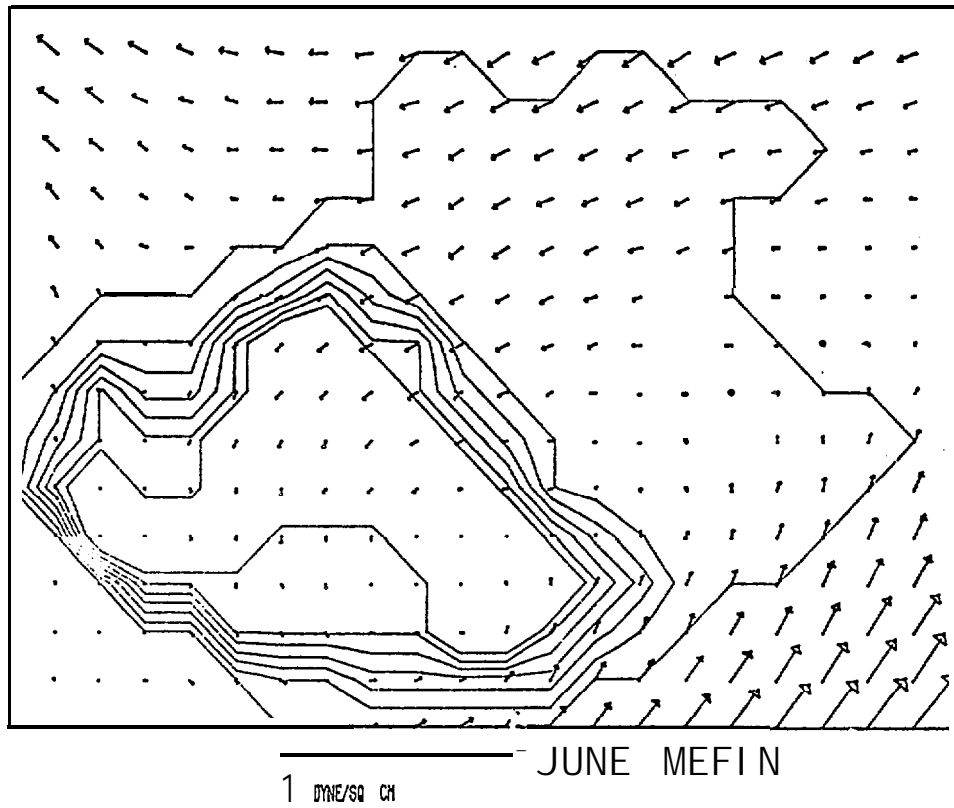


Figure 7

WINDSTRESS VECTOR PLOT

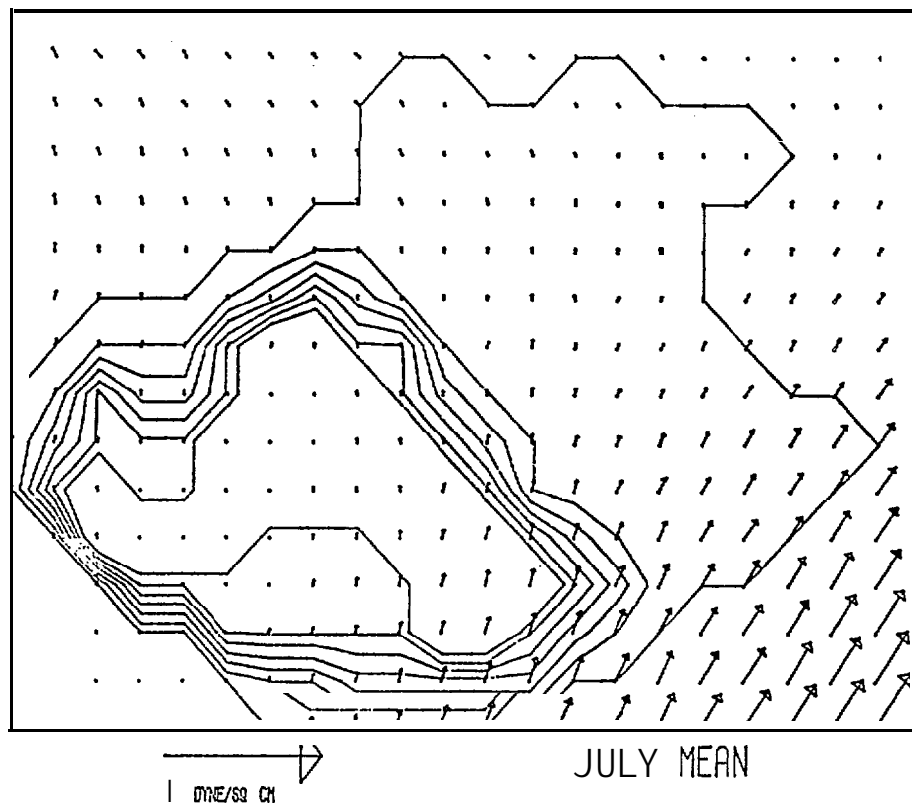


Figure 8

WINDSTRESS VECTOR PLOT

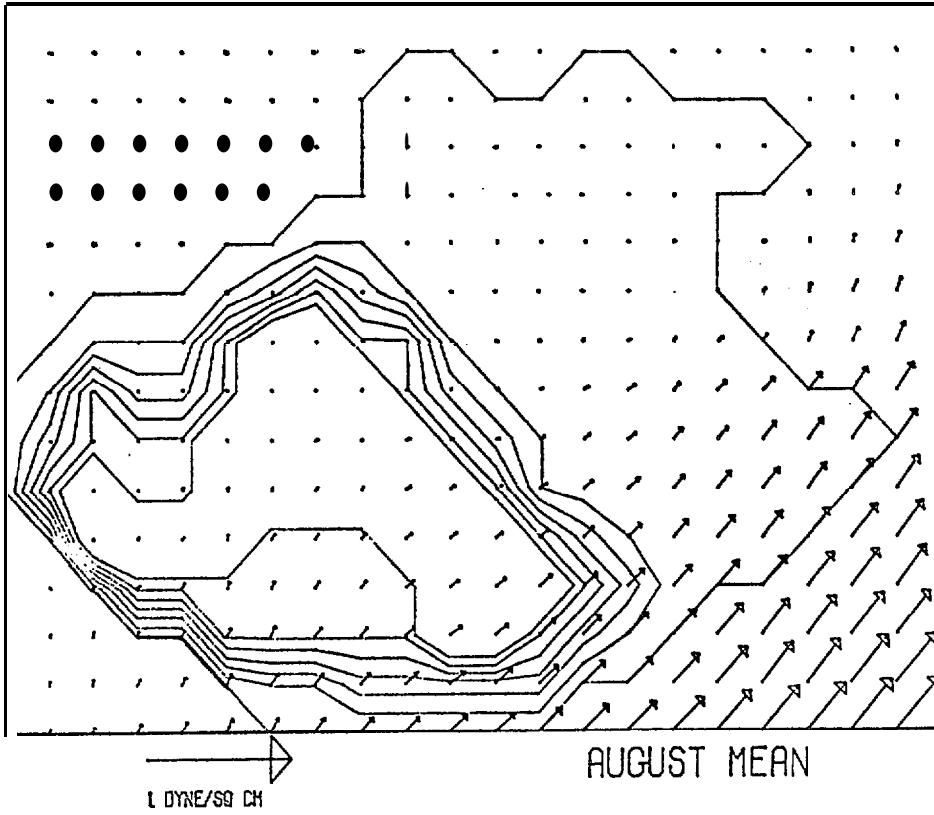


Figure 9

WINDSTRESS VECTOR PLOT

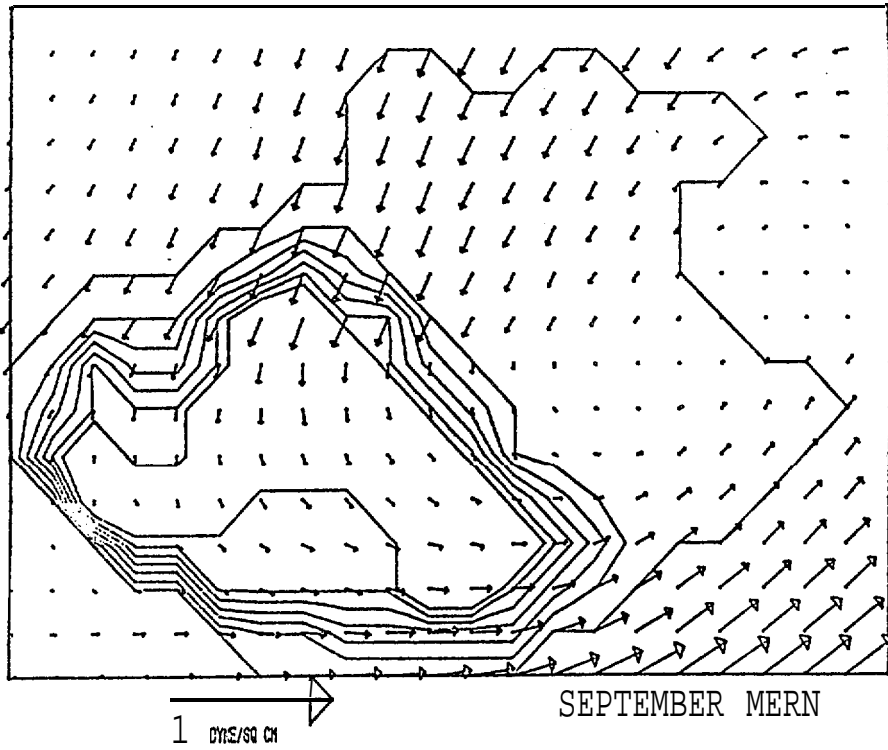


Figure 10

WINDSTRESS VECTOR PLOT

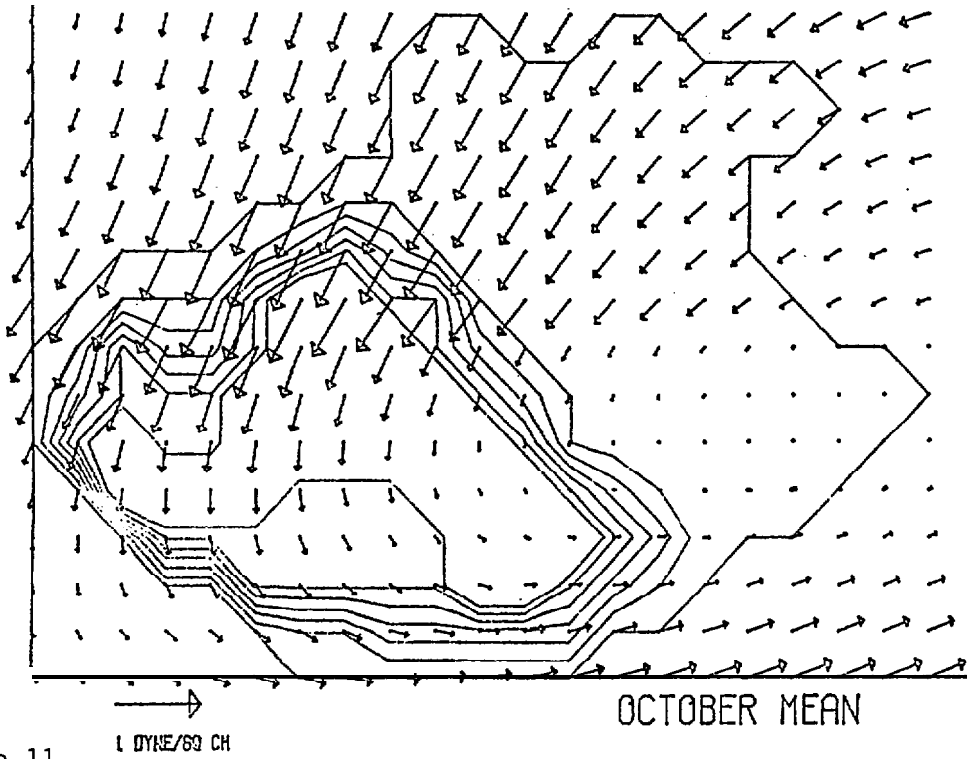


Figure 11

WINDSTRESS VECTOR PLOT

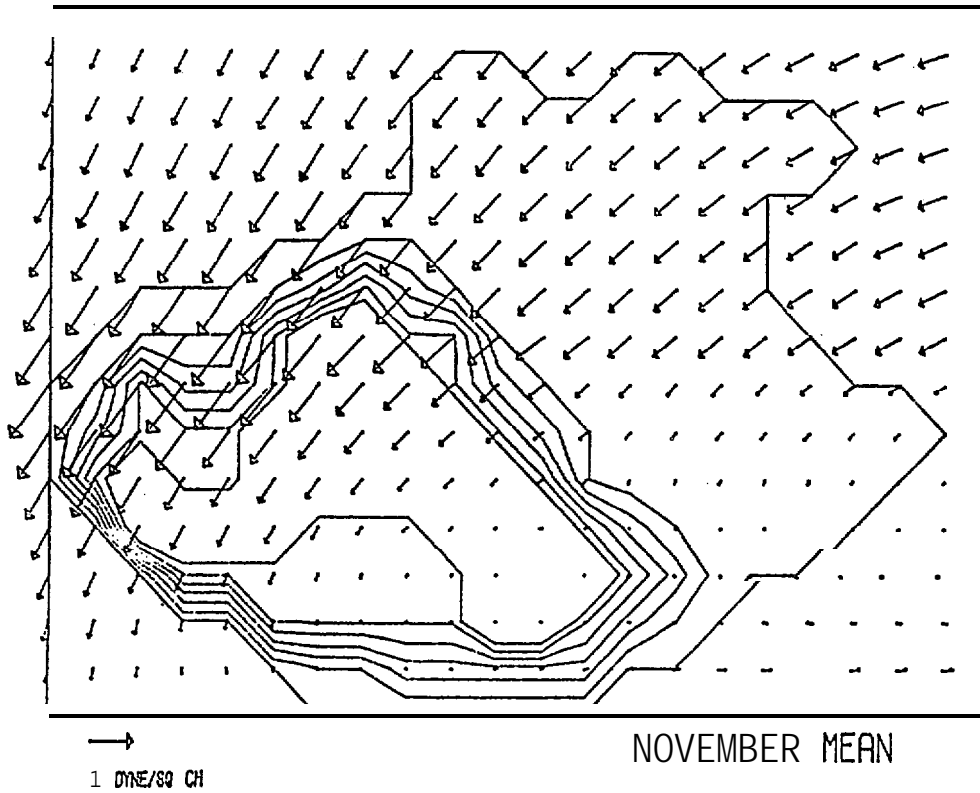


Figure 12

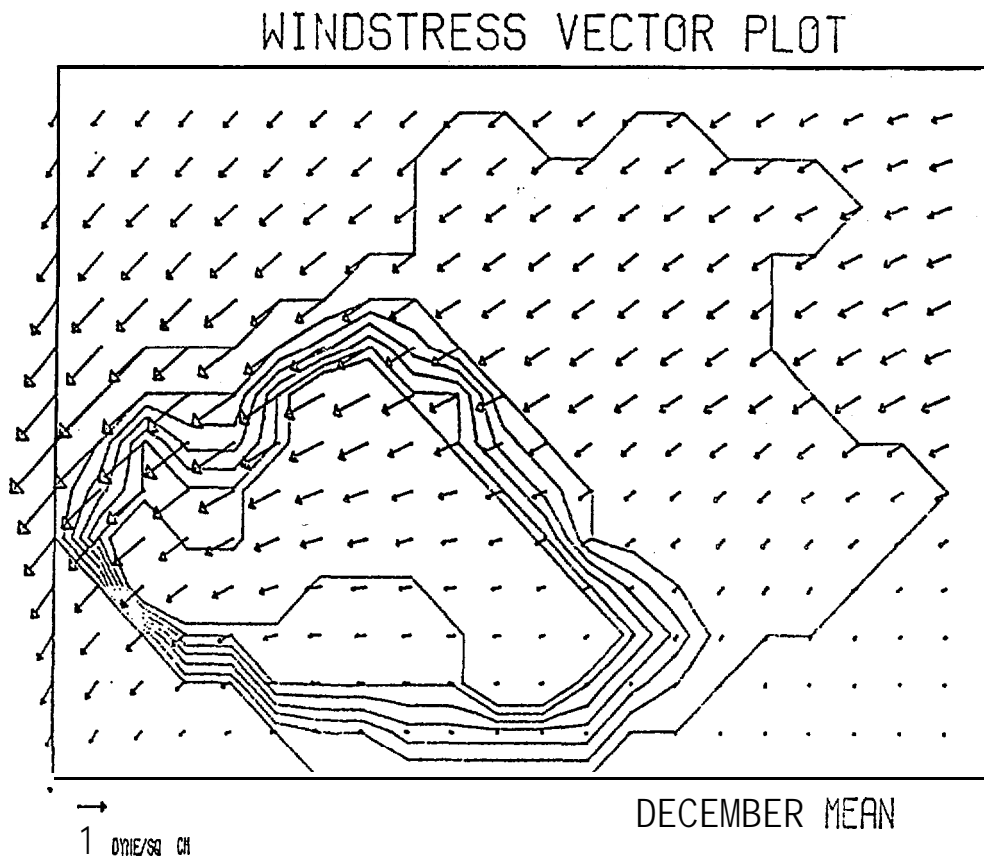


Figure 13

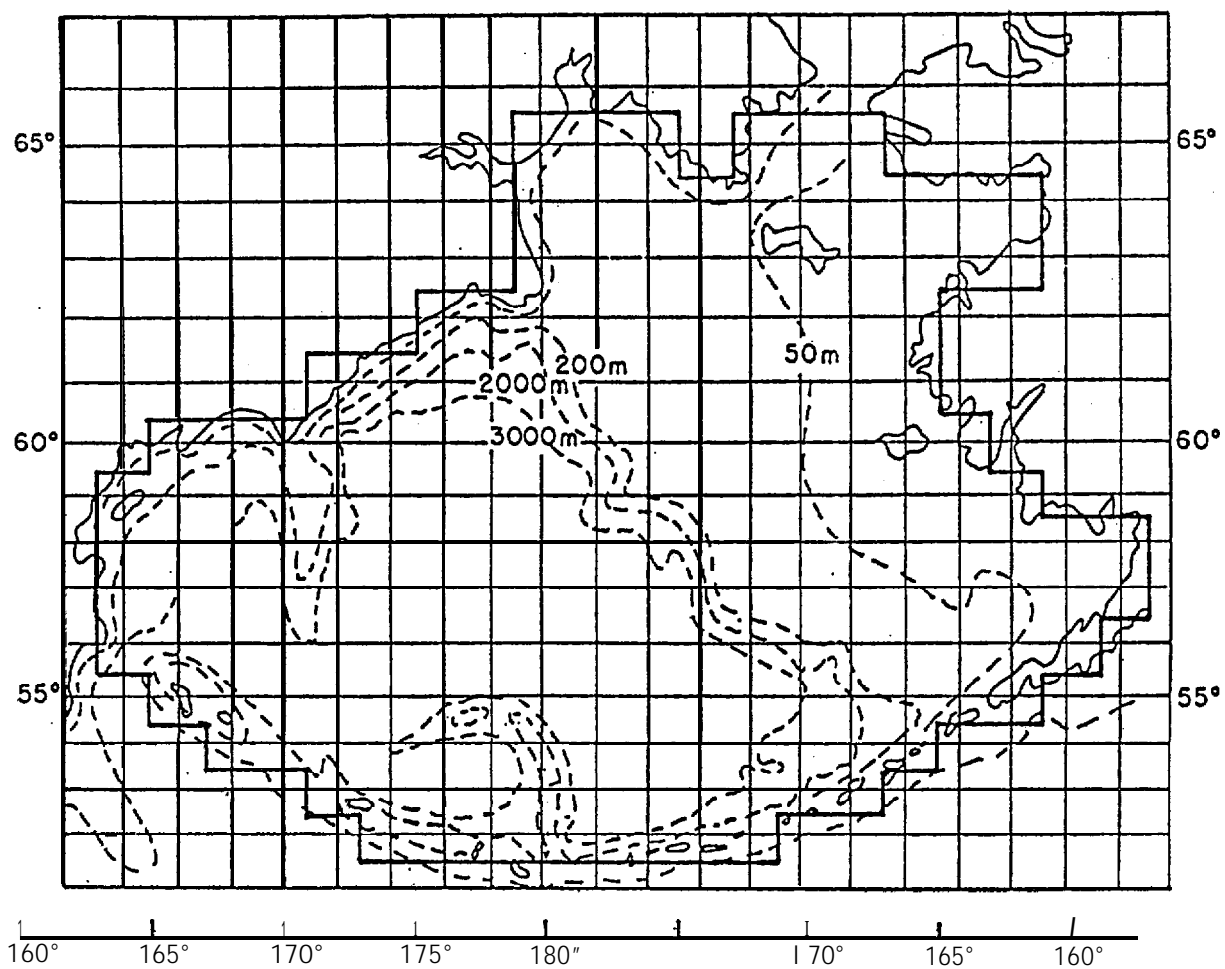


Figure 14

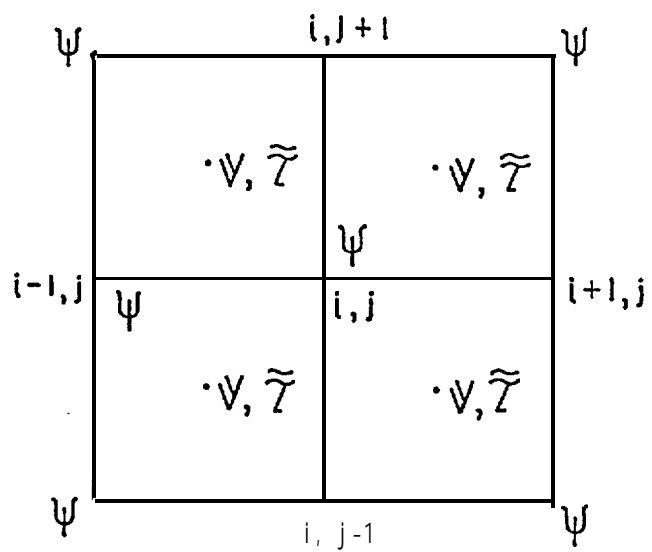


Figure 15

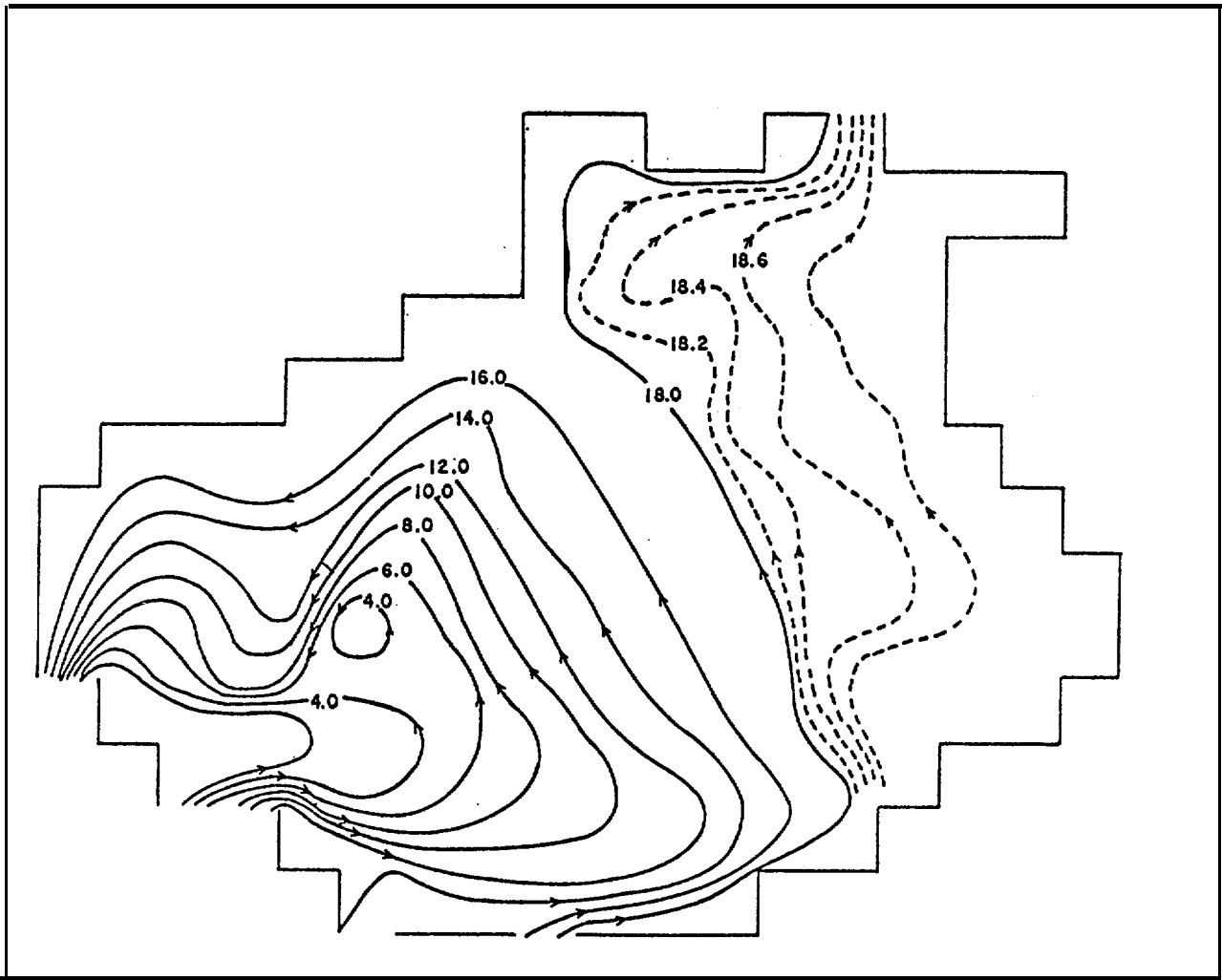


Figure 16

VELOCITY VECTOR PLOT

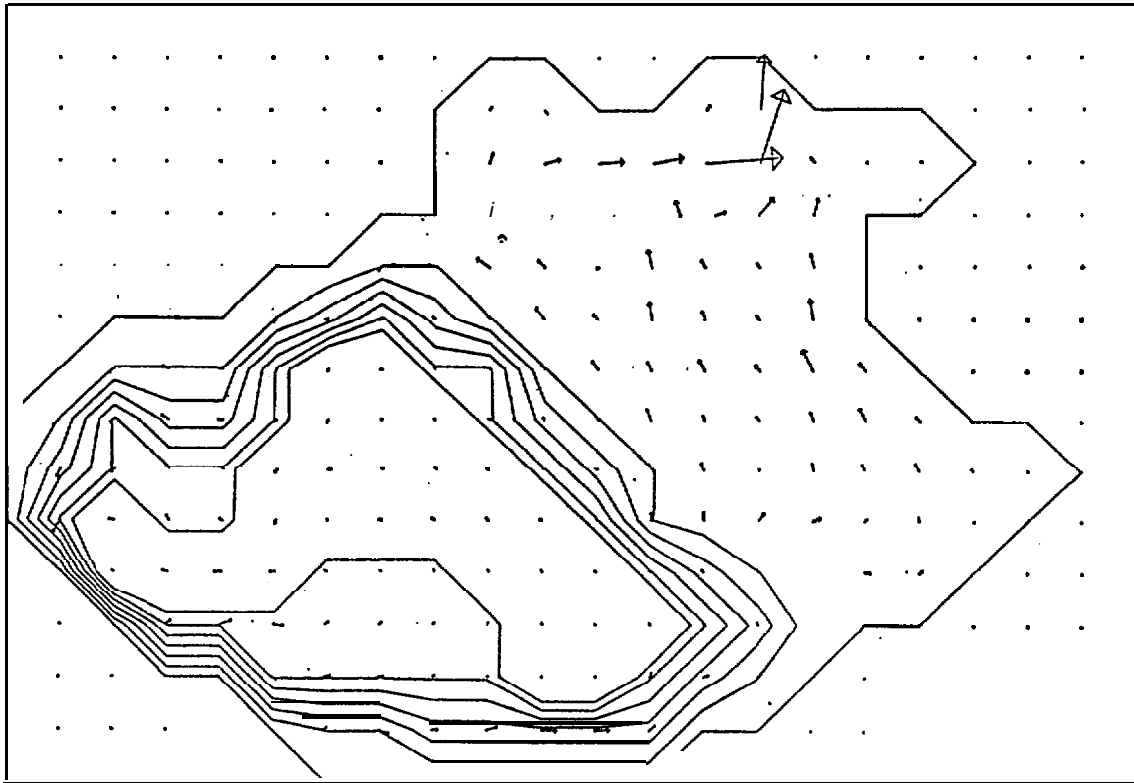


Figure 17 10 (cm/sec)

VELOCITY VECTOR PLOT

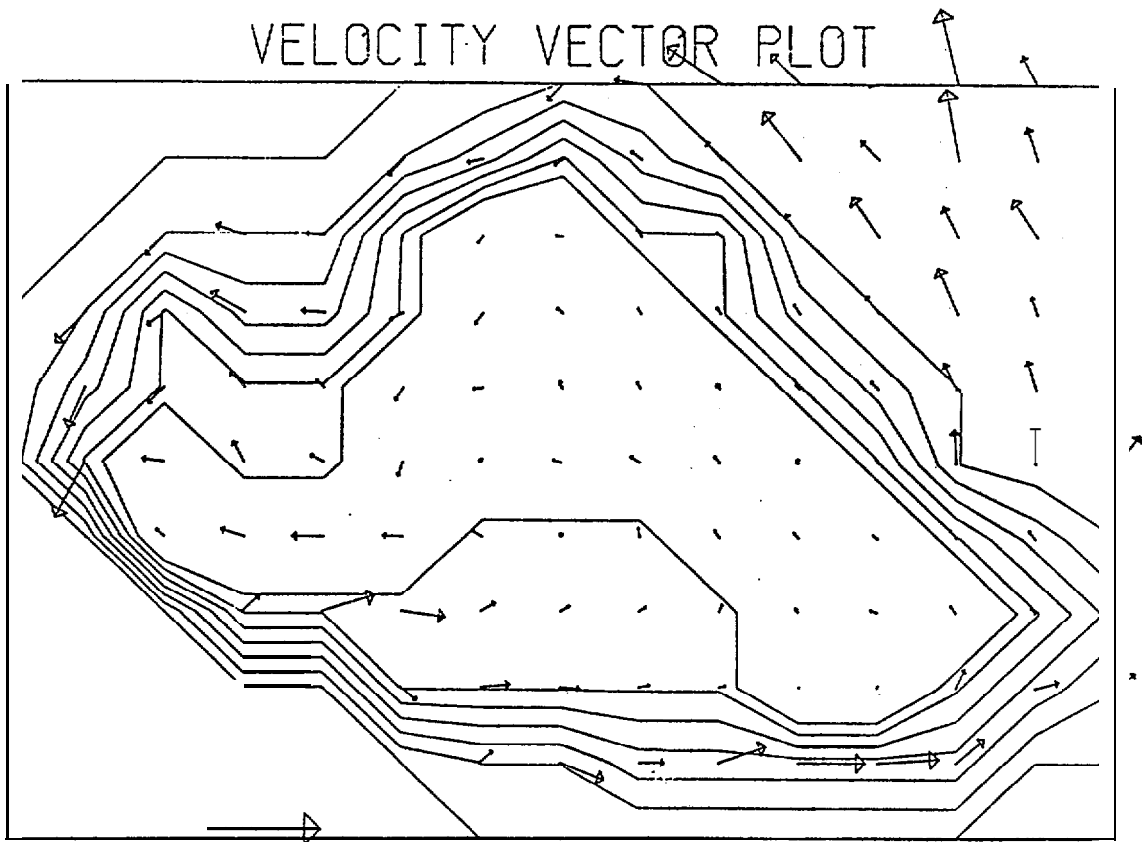


Figure 18

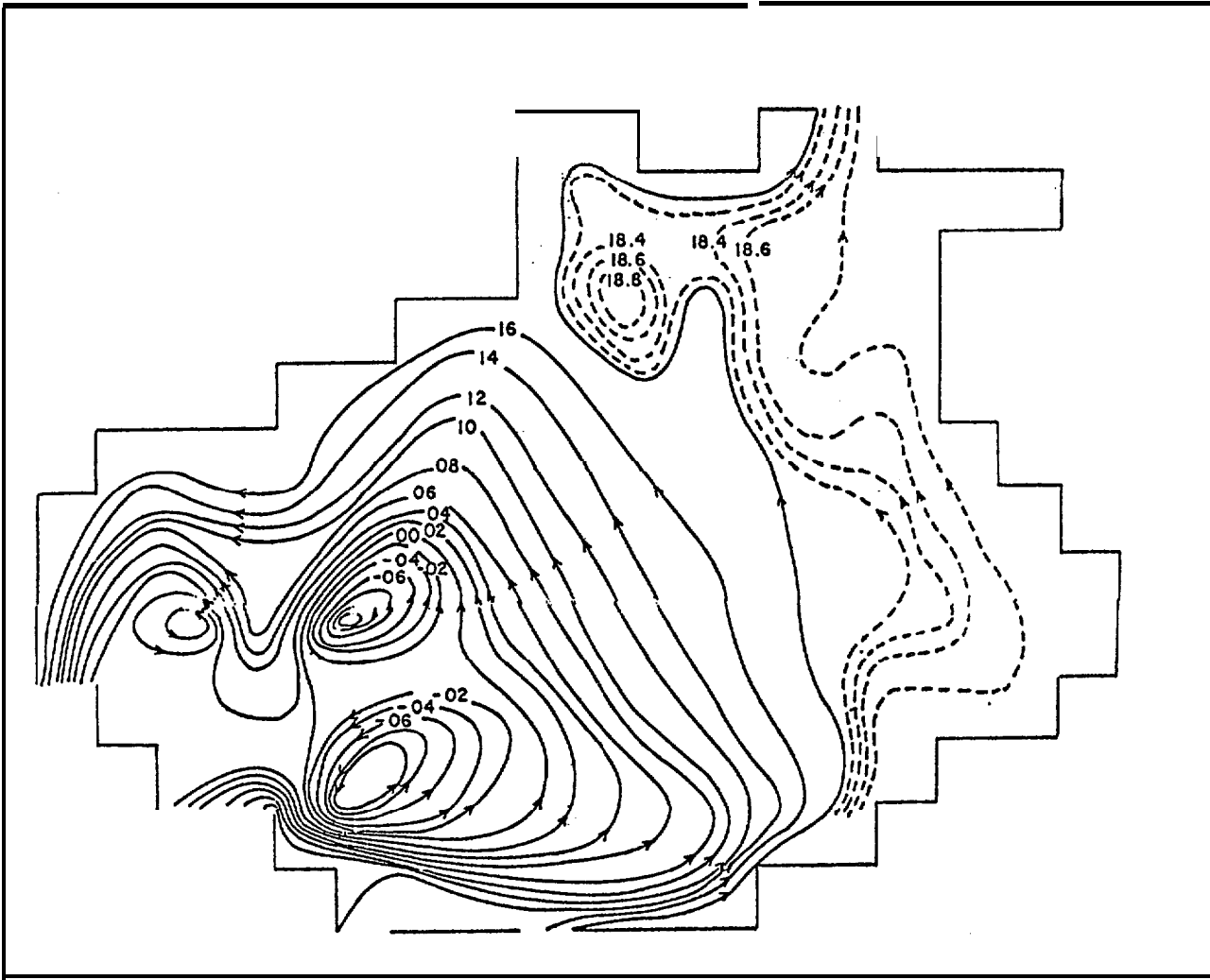


Figure 19

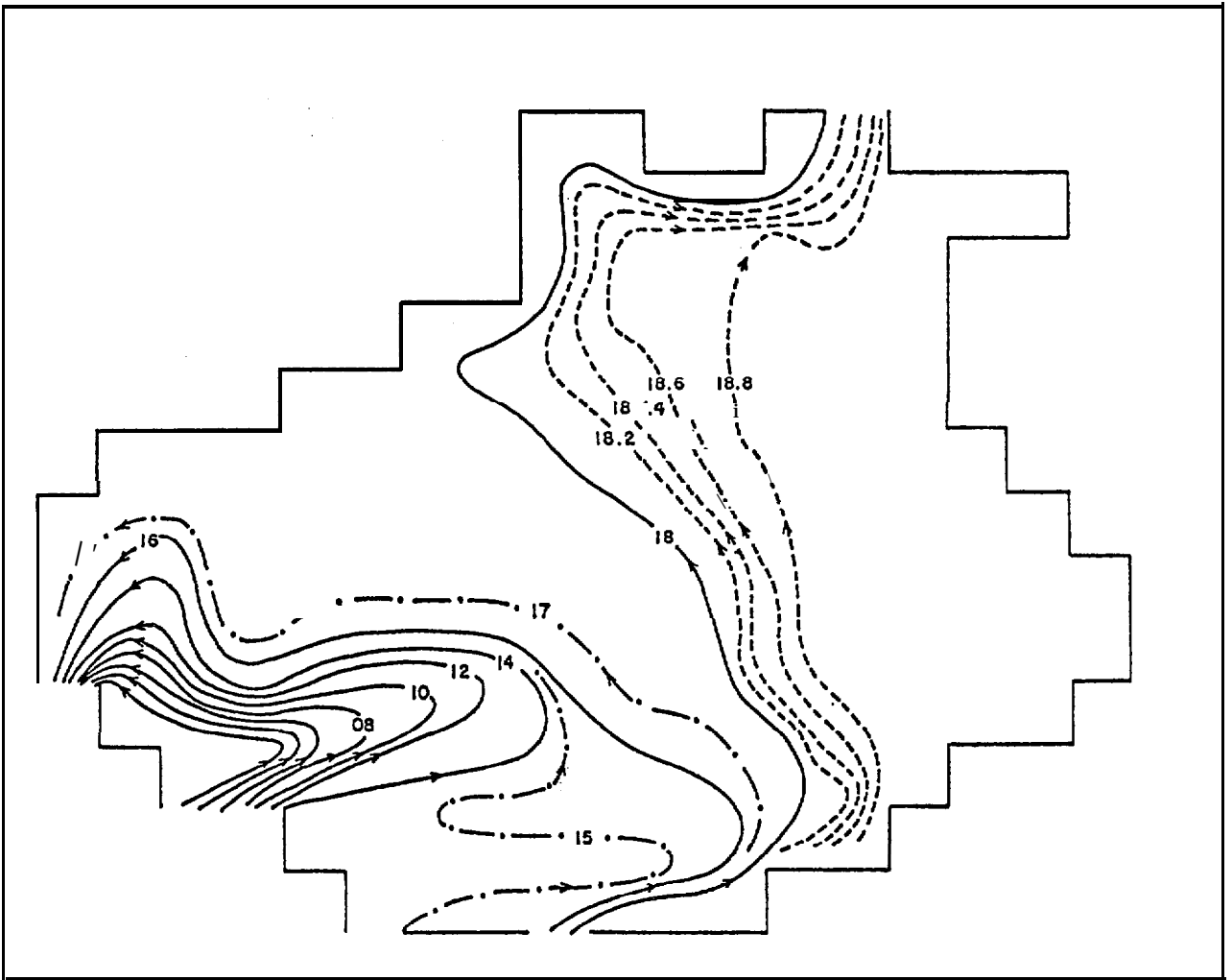


Figure 20

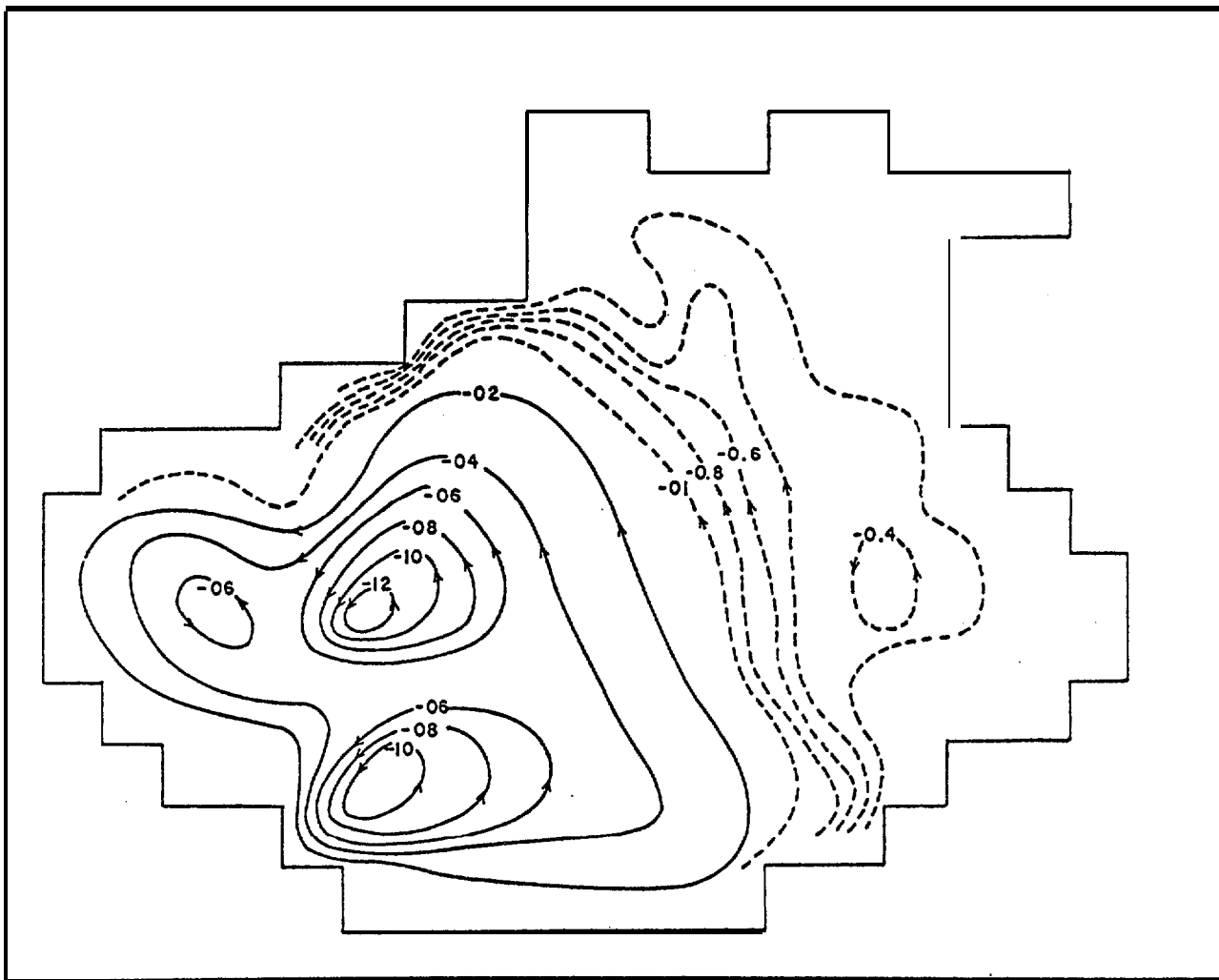


Figure 21

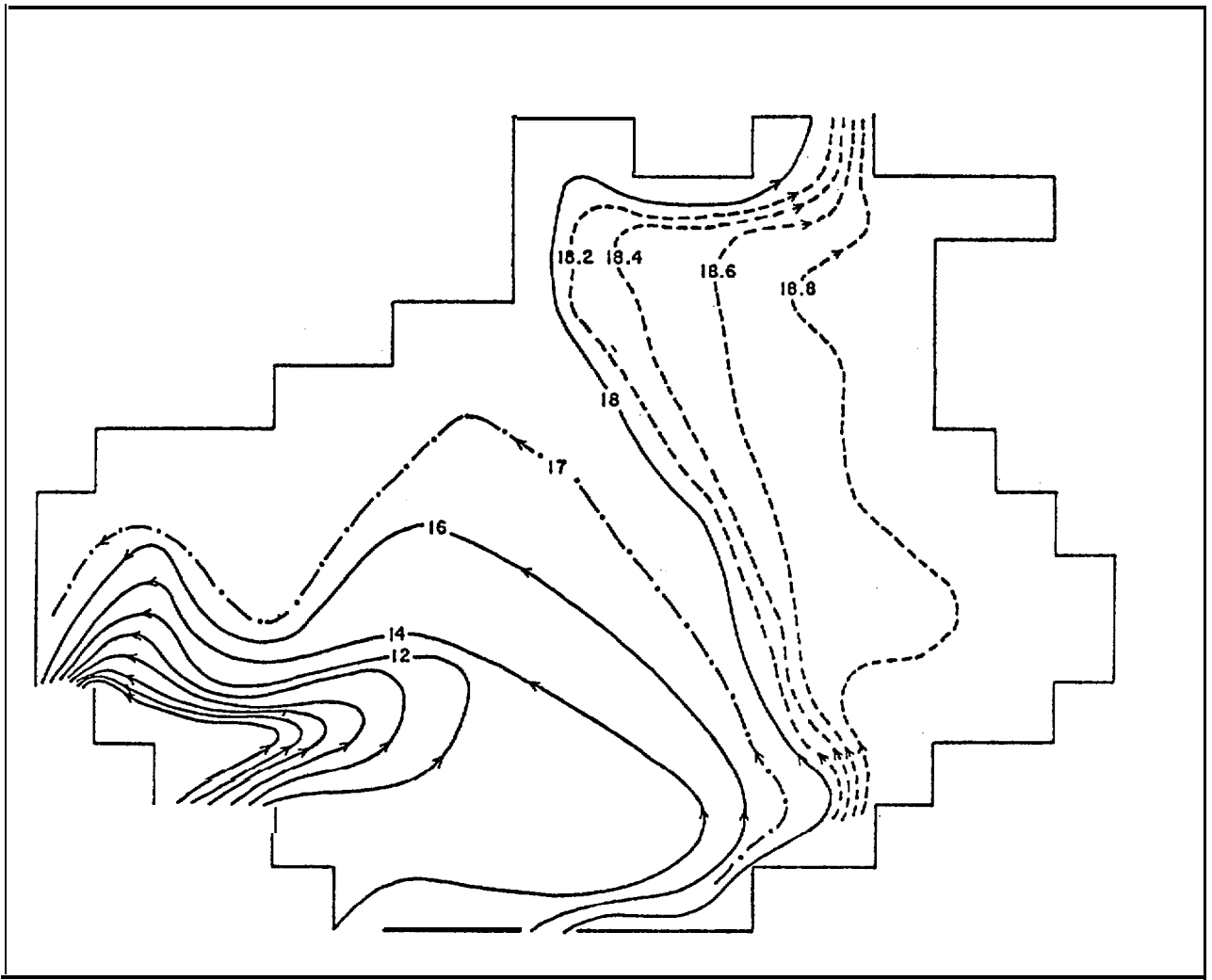


Figure 22

APPENDIX G
Trajectory Model Listing

September 1978

This appendix contains a listing of the trajectory model used to generate the trajectories presented in this report. The code was designed by R.J. Stewart for the NEGQA region and utilizes the environmental library described in the main body of the report.

```

PROGRAM MCTRAJ( INPUT,OUTPUT,TAPE5=INPUT,TAPE6=OUTPUT,
*TAPE1,TAPE2,TAPE3,TAPE8,TAPE9,TAPE17,TAPE23,TAPE29)
      BE CAREFUL TO RESERVE BUFFERS ONLY FOR THOSE FILES BEING USED.
      SUBROUTINES
      CNVWND: CALLED BY MCTRAJ, DECODES INTEGER REPRESENTATION OF
              WIND VECTOR(M/S)
      CNVCUR: CALLED BY MCTRAJ, DECODES INTEGER REPRESENTATION OF
              CURRENT VECTOR(M/S)

      FUNCTIONS
      AVHAG:   RETURNS TWELVE HOURLY AVERAGE MAGNITUDE
      DEGPKM:  RETURNS DEGREES LONGITUDE PER KILOMETER
              AT LATITUDE SPECIFIED IN ARGUMENT

      INPUT DATA SETS
      PATSEQ = SEQUENCE OF WIND PATTERNS? APPENDED TO END OF TAPE3
              ANI) TAPE4.
      WMI694 = MID IS HOURLY DATA JUN-SEP 1974 (INTEGER CODED)
      WMI135 = TAPE3, MID IS HOURLY DATA JAN-MAR 1975 (INTEGER CODED)
      WB125 = EB33 HOURLY DATA JAN-FEB 1975 (INTEGER CODED)
      RUNPFG = TAPE5, INPUT DATA FOR THE MAIN PROGRAM(CARDS,TERM)
      CURM62 = TAPE9, STATION 62 CURRENT METER DATA FEB 1975(INTEGER CODED)
      CURM60 = TAPE9, STATION 60 CURRENT METER DATA JUL 1974(INTEGER CODED)
      WINDXY = TAPE17, WIND PATTERNS FOR NEGQA, 13 TYPES (INTEGER CODED)
      CURRXY = TAPE23, CURRENT PATTERN FOR NEGQA, 13 BAROTROPIC,
              2 BAROCLINIC (INTEGER CODED)
      MAP = TAPE29, DIGITAL COASTLINE REPRESENTATION (0 IS WATER)

      OUTPUT DATA SETS
      NDATA = TAPE2, SPILL TRAJECTORY POSITIONS FOR PLOT VIA PICTUR
      OUTS = TAPE6, LISTING OF PROGRAM

      COMMON/WNDATA/WINDTM
      REAL NCLAT,ECLONG,SCLAT,WCLONG
      INTEGER WINDTM,CURRTM
      DIMENSION MSTIND(3,14)
      INTEGER STRTDA,STRTHR
      INTEGER WINDXY,CURRXY
      DIMENSION TWLTLG(2,2)
      DIMENSION TCLTLG(2,2)
      DIMENSION WINDTM(24,90),CURRTM(24,90)
      DIMENSION MAP(80,40)
      DIMENSION IWNDSEQ(2,90)
      DIMENSION WINDXY(40,20,13),CURRXY(60,30,13)
      DIMENSION X(960),Y(960),YLAT(960),XLONG(960)
      DIMENSION IBAROC(60,30)
      DIMENSION UVCTRW(2,2,13),UVCTRC(2,2,13)
      DIMENSION WMGSTN(13),CMGSTN(13)
      DIMENSION UWSTN(13)
      DIMENSION VWSTN(13)
      DIMENSION UCSTN(13)
      DIMENSION VCSTN(13)
      DATA WDNFAC/.03/
      DATA NCLAT/60.50/,ECLONG/138.00/,SCLAT/58.00/,WCLONG/148.00/
      DATA TWLTLG/59.43,146.33,58.50,141.00/
      DATA TCLTLG/59.55,142.27,60.03,145.85/
      DATA X/960*9999./, Y/960*0.0/

```

```

C           AT THE BEGINNING OF THE PROGRAM AND THE DATA STATEMENTS.
C
DO 10 I=1,90
  READ(3,1040)(WINDTM(J,I),J=1,12)
  READ(3,1040)(WINDTM(J,I),J=13,24)
  READ(9,1045)(CURRTM(J,I),J=1,8)
  READ(9,1045)(CURRTM(J,I),J=9,16)
  READ(9,1045)(CURRTH(J,I),J=17,24)
10 CONTINUE
1040 FORMAT(12I6)
1045 FORMAT(8I8)
C
C           THE LAST RECORDS IN THE WIND TIME SERIES CONTAIN THE
C           PATTERN SEQUENCE
C
  READ(3,1090)((IWNDSEQ(K,J),K=1,2),J=1,30)
  READ(3,1090)((IWNDSEQ(K,J),K=1,2),J=31,60)
  READ(371090)((IWNDSEI3(K,SJ),K=1,2),J=61,90)
1090 FORMAT(30I2)
C
C           THE FOLLOWING ARRAY CONTAINS THE 13 WIND FIELDS
C
DO 15 K=1,13
  DO 14 J=1,20
    DO 13 LL=1,4
      LLO=(LL-1)*10+1
      LHI=LLO+9
      READ(17,2000)(WINDXY(L,J,K),L=LLO,LHI)
    13 CONTINUE
  14 CONTINUE
  15 CONTINUE
2000 FORMAT(10I6)
C
C           THE FOLLOWING ARRAY CONTAINS THE 13 BAROTROPIC CURRENT FIELDS
C
  DO 23 K=1,13
    DO 22 J=1,30
      DO 21 LL=1,6
        LLO=(LL-1)*10+1
        LHI=LLO+9
        READ(23,2002)(CURRXY(L,J,K),L=LLO,LHI)
      21 CONTINUE
    22 CONTINUE
  23 CONTINUE
2002 FORMAT(10I8)
C
C           THE ARRAY IBAROC CONTAINS THE BAROCLINIC COMPONENT OF THE CURRENT
C           FIELD. IT IS ASSUMED CONSTANT OVER THE SIMULATION PERIOD,
C
  IREAD = 0
  DO 29 J=1,30
    DO 28 LL=1,6
      LLO = (LL-1)*10+1
      LHI = LLO+9
      READ(23,2002)(IBAROC(L,J),L=LLO,LHI)
    28 CONTINUE
  29 CONTINUE

```

```

IYBGN = MSTIND(IROW,1)
IDABGN = MSTIND(IROW,2)
IHRBGN = MSTIND(IROW,3)
IYREND = MSTIND(IROW,4)
IMOEND = MSTIND(IROW,5)
IDAEND = MSTIND(IROW,6)
IHREND = MSTIND(IROW,7)
LASTDA = MSTIND(IROW,8)
NOWSTN = MSTIND(IROW,9)
NOCSTN = MSTIND(IROW,10)
NBAROC = MSTIND(IROW,11)

C
C      CHECK IF START IS EARLIER THEN DATA
C      IF(STRTDA.LT.MSTIND(IROW,8))GOTO 490
C
C      NOWWRITE ALL PERTINENT DATA READ FROM TAPE 5 AT TOP OF NEW PAGE
C      ON TAPE6.
C
WRITE(6TIO10)
WRITE(6J1017)MSTIND(IROW,1) ,MSTIND(IROW,2),MSTIND(IROW,3),
1 MSTIND(IROW,4)
WRITE(6,1018)MSTIND(IROW,5),MSTIND(IROW,6),MSTIND(IROW,7),
P 2 MSTIND(IROW,8)
WR11E(15J1027) IDASEP,IHRSEP
WRITE(6,1067)STRTDA,STRTHR
WRITE(6,991)MSTIND(IROW,9),MSTIND(IROW,10)
991 FORMAT(1X,*EARLIEST START. POSSIBLE*,3X,* STRTDA = *,
1 I2,2X,*STRTHR = *,I2)
WRITE(6,1068)LASTDA
WRITE(6,1037)SRCLAT,SRCLNG
WRITE(6,1072)NOWSTN,TWLTG(1,NOWSTN),TWLTG(2,NOWSTN)
WRITE(6,1073)NOCSTN,TCLTLG(1,NOCSTN),TCLTLG(2,NOCSTN)
WRITE(6,1074)NBAROC
1010FORMAT(1H1,* SIMULATION DATA CHOSEN IS: */)
1015 FORMAT(4(1X,I2))
1017 FORMAT(* IYBGN = *,I2,2X,*IMOEND = *,I2,2X,*IDABGN = *,
* I2,2X,*IHRBGN = *,I2)
1018 FORMAT(* IYREND = *,I2,2X,*IMOEND = *,I2,2X,*IDAEND = *,
* I2,2X,*IHREND = *,I2)
1025 FORMAT(7X,2(I2,1X))
1027 FORMAT(27X,* IDASEP = *,I2,
12X,*IHRSEP = *,I2)
1035 FORMAT(1X,F7.4,4X,F8.4)
1037 FORMAT(* SRCLAT = *,F7.4,2X,*SRCLNG = *,F8.4)
1067 FORMAT(5X,*FOR THIS RUN*,10X,* STRTDA = $,I2,2X,
1 *STRTHR = *,I2)
1048 FORMAT(5X,*LAST POSSIBLE DATE*,4X,*LASTDA = *,I2)
1070 FORMAT(2X,3(I2,2X))
1072 FORMAT(* WIND STATION NO = *,I2,* (MID IS = 1, EB33 = 2)*,
*2X,*AT LAT = *,F7.3,2X,*LONG = *,F7.3)
1073 FORMAT(* CURRENT STATION NO = *,I2,1X,* (62 = 1, 60 = 2)*,
*2X,*AT LAT = *,F7.3,2X,*LONG = *,F7.3)
1074 FORMAT(* INDEX OF BAROCLINIC FIELD = *,I2,5X,
** (1 = JULY 1974, 2 = FEBRUARY 1975)*)
C      THE FOLLOWING ARRAYS CONTAIN THE CURRENT AND WIND TIME SERIES. THE
C      VARIABLE TAPE NUMBER IDENTIFIES THE SOURCE PER THE COMMENTS

```



```

29 CONTINUE
  IREAD = IREAD+1
  IF(IREAD, EQ, 1, AND, NBAROC, EQ, 2) GOTO 27
  DO 31 J=1, 40
    READ(29, 2050)(MAP(I, J), I=1, 80)
31 CONTINUE
  WRITE(6, 2060)
  DO 32 J=1, 40
    JJ=41-J
    WRITE(6, 2055)(MAP(I, JJ), I=1, 80)
32 CONTINUE
2050 FORMAT(80I1)
2055 FORMAT(1X, 80I1)
2060 FORMAT(20X, *MAP*)
C
C          CALCULATE INDICES OF WIND AND CURRENT METER STATIONS
C
  JWSTN = IFIX((TWLTLG(1, NOWSTN)-SCLAT)*20/(NCLAT-SCLAT))+1
  IWSTN = IFIX((WCLONG-(TWLTLG(2, NOWSTN)))*40/(WCLONG-ECLONG))+1
  JCSTN = IFIX((TCLTLG(1, NOCSTN)-SCLAT)*30/(NCLAT-SCLAT))+1
  ICSTN = IFIX((WCLONG-(TCLTLG(2, NOCSTN)))*60/(WCLONG-ECLONG))+1
  WRITE(6, 2074)
2074 FORMAT(1H0, * INDICES OF WIND AND CURRENT METER STNS ARE: *//)
  WRITE(6, 2075) IWSTN, JWSTN, ICSTN, JCSTN
2075 FORMAT(* IWSTN = *, I2, 2X, * JWSTN = *, I2, 2X, * ICSTN = *,
*          I2, 2X, * JCSTN = *, I2)
"
C          CALCULATE THE NOMINAL WIND AND CURRENT VELOCITIES FOR THE 13
E          PATTERN TYPES AT THE WIND AND CURRENT METER STATIONS,
C          ALSO DETERMINE THE WIND AND CURRENT MAGNITUDES AND THE
L          REQUIRED LONGITUDINAL AND TRANSVERSE UNIT VECTORS.

  WRITE(6, 2079)
  CALL CNVCUR( IBAROC(ICSTN, JCSTN), UBCSTN, VBCSTN)
  WRITE(6, 5050) UBCSTN, VBCSTN
5050 FORMAT(* UBCSTN = *, E12.4, 2X, * VBCSTN = *, E12.4)
  110 50 J=1, 13
    CALL CNVWND(WINDXY(IWSTN, JWSTN, J), UWSTN(J), VWSTN(J))
    CALL CNVCUR(CURRXY(ICSTN, JCSTN, J), UCSTN(J), VCSTN(J))
    WIND AND CURRENT VECTOR MAGNITUDE
    WMGSTN(J) = SQRT((UWSTN(J)**2)+(VWSTN(J)**2))
    CMGSTN(J) = SQRT((UCSTN(J)**2)+(VCSTN(J)**2))
    WIND UNIT VECTOR ARRAY
    UVCTRW(1, 1, J) = UWSTN(J)/WMGSTN(J)
    UVCTRW(2, 1, J) = VWSTN(J)/WMGSTN(J)
    UVCTRW(1, 2, J) = -VWSTN(J)/WMGSTN(J)
    UVCTRW(2, 2, J) = UWSTN(J)/WMGSTN(J)
    CURRENT UNIT VECTOR ARRAY
    UVCTRC(1, 1, J) = UCSTN(J)/CMGSTN(J)
    UVCTRC(2, 1, J) = VCSTN(J)/CMGSTN(J)
    UVCTRC(1, 2, J) = -VCSTN(J)/CMGSTN(J)
    UVCTRC(2, 2, J) = UCSTN(J)/CMGSTN(J)
2079 FORMAT(1H0, * WIND AND CURRENT PATTERN DATA AT STATIONS *//)
  WRITE(6, 2080) J, WINDXY(IWSTN, JWSTN, J),
*          CURRXY(ICSTN, JCSTN, J)

```

```

        WRITE(6,2082)UWSTN(J),VWSTN(J),
*           UCSTN(J),VCSTN(J),
*           WMGSTN(J),CMGSTN(J)
50 CONTINUE
    WRITE(6,2090)
    DO 51 I=1,13
        WRITE(6,2092)((UVCTRW(1,K,I),K=1,2),
*                   (UVCTRC(1,K,I),K=1,2))
        WRITE(6,2092)((UVCTRW(2,K,I),K=1,2),
*                   (UVCTRC(2,K,I),K=1,2))
51 CONTINUE
    CALL CNVCUR(IBAROC(ICSTN,JCSTN),UBCSTN,VBCSTN)
2080 FORMAT(* J=*,I2,5X,*WINDXY=*,I6,2X,*CURRXY=*,I8)
2082 FORMAT(* UWSTN=*,E12.4,2X,*VWSTN=*,E12.4,2X,* UCSTN=*,E12.4,
*           2X,*VCSTN=*,E12.4,2X,* WMGSTN=*,E12.4,2X,*CMGSTN=*,E12.4)
2090 FORMAT(20X,*WIND AND CURRENT UNIT VECTOR ARRAY*)
2092 FORMAT(1X,4(E12.4,2X))
C
    WRITE(2,2093)SCLAT,WCLONG,NCLAT,ECLONG
2093 FORMAT(4(1X,F9.4))
C
C     INITIALIZE TIME COUNTER
    IHR = STRTHR
    IDA = STRTDA
100 ISEQNM = 1
    ISEQDA = IDA
C
C     BEGIN TRAJECTORY CALCULATIONS
C
    IF(IHR.LE.6.OR.IHR.GT.18)GOTO 101
    ISEQNM = 2
    GOTO 104
101 IF(IHR.LE.6)GOTO 104
    ISEQDA = IDA + 1
104 WNDMAG = AVMAG(ISEQNM,ISEQDA)
    XLONG(1) = SRCLNG
    YLAT(1) = SRCLAT
    X(1) = (WCLONG-SRCLNG)/DEGPKM(SRCLAT)
    Y(1) = (SRCLAT-SCLAT)/DGPKM
    WRITE(6,2999)
2999 FORMAT(1H0,* TRAJECTORY DATA */)
    WRITE(6,3000)X(1),Y(1),XLONG(1),YLAT(1)
3000 FORMAT(* X=*,F8.2,1X,*Y=*,F8.2,1X,*XLONG=*,F8.2,1X,*YLAT=*,F8.2)
    KOUNTI = 1
C
C     THE PROBLEM IS NOW INITIALIZED.  BEGIN CALCULATING
C     CONSECUTIVE POSITIONS
C
    DO 120 I=2,959
    IW = IFIX(((WCLONG-XLONG(I-1))*40)/(WCLONG-ECLONG))+1
    JW = IFIX(((YLAT(I-1)-SCLAT)*20)/(NCLAT-SCLAT))+1
    ICR = IFIX(((WCLONG-XLONG(I-1))*60)/(WCLONG-ECLONG))+1
    JCR = IFIX(((YLAT(I-1)-SCLAT)*30)/(NCLAT-SCLAT))+1
    IMAP = IFIX(((WCLONG-XLONG(I-1))*80)/(WCLONG-ECLONG))+1

```

```

      JMAP = TETX(((YLAT(I-1)-SCLAT)*40)/(NCLAT-SCLAT))+1
      WRITE(6,3020)IW,JW,ICR,JCR,JMAP,JMAP,IDA,IHR
3020 FORMAT(* IW=*,I2,2X,*JW=*,I2,2X,*ICR=*,I2,2X,*JCR=*,I2,2X,
*          *JMAP=*,I2,2X,*JMAP=*,I2,2X,*IDA =*,I3,2X,*IHR=*,I2)
C
C      GROUNDING CHECK
C      IF(MAP(IMAP,JMAP).NE.0) GOTO 140
C      WIND ARRAY CHECK
C      IF(WINDXY(IW,JW).LT.0) GOTO 140
C      CURRENT ARRAY CHECK
C      IF(CURRXY(ICR,JCR).LT.0) GOTO 140
C      DETERMINE IF BAROCLINIC CURRENT IS KNOWN
C      IF(IBAROC(ICR,JCR).LT.0) GOTO 140
C      DETERMINE LOCAL BAROCLINIC CURRENT VELOCITY
C      CALL CNVCUR(IBAROC(ICR,JCR),BCUC,BCVC)
C      CHECK FOR BAD DATA
C      IF(IWINDSEQ(ISEQNM,ISEQDA).LT.0) GOTO 450
C      LOOK-UP PATTERN NUMBER TYPE
C      NUMSEQ = IWINDSEQ(ISEQNM,ISEQDA)
C      DETERMINE LOCAL BAROTROPIC CURRENT VELOCITY
C      CALL CNVCUR(CURRXY(ICR,JCR,NUMSEQ),BTUC,BTVC)
C      DETERMINE LOCAL WIND VELOCITY
C      CALL CNVWIND(WINDXY(IW,JW,NUMSEQ),WUC,WVC)
C      DETERMINE STRENGTH OF WIND FIELD
C      FLDSTR = WNDMAG/WMGSTN(NUMSEQ)
C      CHECK FOR BAD DATA
C      IF(WINDTM(IHR,IDA).LT.0) GOTO 450
C      DETERMINE HOURLY WIND VELOCITY AT WIND STATION
C      CALL CNVWIND(WINDTM(IHR,IDA),UWHR,VWHR)
C      DETERMINE WIND PERTURBATION VELOCITY AT WIND STATION
C      UWPERT = UWHR - FLDSTR*UWSTN(NUMSEQ)
C      VWPERT = VWHR - FLDSTR*VWSTN(NUMSEQ)
C      DECOMPOSE INTO ALONG AND LEFT PERPENDICULAR COMPONENTS
C      WALNGU = UVCTRW(1,1,NUMSEQ)*UWPERT + UVCTRW(2,1,NUMSEQ)*VWPERT
C      WLEFTU = UVCTRW(1,2,NUMSEQ)*UWPERT + UVCTRW(2,2,NUMSEQ)*VWPERT
C      DETERMINE LOCAL WIND SPEED FOR TURBULENCE SCALE
C      WMGLOC = SQRT((WUC**2) + (WVC**2))
C      TRBSCL IS NOW THE FOLLOWING RATIO OF THE UNWEIGHTED FIELD VARIABLES
C      TRBSCL = WMGLOC/WMGSTN(NUMSEQ)
C      WALNGU = WALNGU*TRBSCL
C      WLEFTU = WLEFTU*TRBSCL
C      CALCULATE X,Y COMPONENTS OF ROTATED PERTURBATION VELOCITY
C      UWPERT = (WALNGU*WUC/WMGLOC) - (WLEFTU*WVC/WMGLOC)
C      VWPERT = (WALNGU*WVC/WMGLOC) + (WLEFTU*WUC/WMGLOC)
C      DETERMINE SYNTHESIZED LOCAL HOURLY WIND VELOCITY
C      WU = FLDSTR*WUC + UWPERT
C      WV = FLDSTR*WVC + VWPERT
C      CHECK FOR BAD DATA
C      IF(CURRTM(IHR,IDA).LT.0) GOTO 450
C      DETERMINE HOURLY CURRENT VELOCITY AT CURRENT STATION
C      CALL CNVCUR(CURRTM(IHR,IDA),UCHR,VCHR)
C      DETERMINE CURRENT PERTURBATION VELOCITY AT CURRENT STATION
C      UCPERT = UCHR - UBCSTN - (FLDSTR**2)*UCSTN(NUMSEQ)
C      VCPERT = VCHR - VBCSTN - (FLDSTR**2)*VCSTN(NUMSEQ)
C      DECOMPOSE INTO ALONG AND LEFT PERTURBATION COMPONENTS

```

```

CALNGU = UVCTRC(1,1,NUMSEQ)*UCPERT + UVCTRC(2,1,NUMSEQ)*VCPERT
CLEFTU = UVCTRC(1,2,NUMSEQ)*UCPERT + UVCTRC(2,2,NUMSEQ)*VCPERT
      DETERMINE LOCAL BAROTROPIC CURRENT MAGNITUDE
CMGLDC = SQRT((BTUC**2) + (BTVC**2))
TRBSCL = CMGLDC/CMGSTN(NUMSEQ)
      DETERMINE SCALED PERTURBATION COMPONENTS
CALNGU = TRBSCL*CALNGU
CLEFTU = TRBSCL*CLEFTU
      CALCULATE SYNTHESIZED LOCAL CURRENT PERTURBATION
UCPERT = (CALNGU*BTUC/CMGLDC) - (CLEFTU*BTVC/CMGLDC)
VCPERT = (CALNGU*BTVC/CMGLDC) + (CLEFTU*BTUC/CMGLDC)
      DETERMINE SYNTHESIZED LOCAL CURRENT VELOCITY.
      THE BAROCLINIC AND PERTURBATION COMPONENTS ARE SCALED
      ALREADY, BUT THE BAROTROPIC PORTION STILL REQUIRES AMPLIFICATION
CU = BCUC + UCPERT + (FLDSTR**2)*BTUC
CV = BCVC + VCPERT + (FLDSTR**2)*BTVC
      STORE VELOCITY DATA IN TAPE 8 FOR STICK VECTOR DRAWINGS
      U1=UCHR*100,
      U2=BCUC*100.
      U3=CU*100,
      V1=VCHR*100,
      V2=BCVC*100.
      V3=CV*100.
      WRITE(8,3029)U1,V1,UWHR,VWHR,U2,V2,U3,V3,WU,WV
3029 FORMAT(10F8.3)
      WRITE MISC. VARIABLES FOR DEBUG
      WRITE(6,3030)CU,CV,WU,WV,BCUC,BCVC,BTUC,BTVC,
      * CALNGU,CLEFTU,TRBSCL,FLDSTR
3030 FORMAT(IX?12E10.3)
      NOW UPDATE POSITION
      X(I) = X(I-1) + 3.6*(CU + WNDFAC*WU)
      Y(I) = Y(I-1) + 3.6*(CV + WNDFAC*WV)
      YLAT(I) = YLAT(I-1) + (Y(I)-Y(I-1))*DGPKM
      XLONG(I) = XLONG(I-1) - (X(I)-X(I-1))*DEGPKM*(YLAT(I))
      UPDATE KOUNTI TO INDICATE NEW POSITION DATA
      KOUNTI = 1
      NOW UPDATE TIME
      IHR = IHR + 1
      IF(IHR.LE.24) GOTO 110
      IDA = IDA + 1
      IHR = IHR - 24
110 IF(IDA.GT.LASTDA) GOTO 140
      IF(IDA.EQ.LASTDA,AND,IHR.GT.18) GOTO 140
      WRITE(6,3040)X(I),Y(I),I
3040 FORMAT(1X,*X(I)=*,FB.2,2X,*Y(I)=*,FB.2,2X,*I=*,I3)
      IF(IHR.NE.7) GOTO 112
      ISEQNM = 2
      WNDMAG = AVMAG(ISEQNM, ISEQDA)
      GOTO 120
112 IF(IHR.NE.19) GOTO 120
      ISEQNM = 1
      ISEQDA = IDA + 1
      WNDMAG = AVMAG(ISEQNM, ISEQDA)
120 CONTINUE
140 WRITE(6,3044)
3044 FORMAT(1H0,* FORMATTED LISTING OF TAPE 2 DATA *//)

```

```

WRITE(6,3045)SCLAT,WCLONG,NCLAT,ECLONG
3045 FORMAT(1X,*SCLAT=*,F8.2,2X,*WCLONG=*,F8.2,2X,*NCLAT=*,F8.2,2X,
* *ECLONG=*,F8.2)
KOUNTI = KOUNTI + 1
DO 142 I=1, KOUNTI
WRITE(2,3050)X(I),Y(I)
WRITE(6,3055)X(I),Y(I)
3050 FORMAT(2(1X,F8.2))
3055 FORMAT(1X,*X(I)=*,F8.2,2X,*Y(I)=*,F8.2)
142 CONTINUE
STRTHR = STRTHR + IHRSEP
STRTDA = STRTDA + IDASEP
IF(STRTHR,LE,24) GO TO 143
STRTDA = STRTDA + 1
STRTHR = STRTHR - 24
143 IF((STRTDA,GT,LASTDA),OR.(STRTDA,EQ,LASTDA,AND,STRTHR,GT,18))
GO TO 500
IDA = STRTDA
IHR = STRTHR
DO 144 I=1,960
X(I) = 9999.
Y(I) = 0.0
144 CONTINUE
GOTO 100

C
C
450 WRITE(6,4010)
4010 FORMAT(1X,*TIME SERIES DATA ERROR SEE LISTING *)
WRITE(6,4020)ISEQNM,ISEQDA,IHR,IDA
4020 FORMAT(1H0,* ISEQNM *,I4,* ISEQDA *,I4,* IHR *,
1 I4,* IDA *,I4/)
C PPRINT OUT DATAFIELDS
DO 455 I=1,90
WRITE(6,4030)(WINDTM(J,I),J=1,12)
WRITE(6,4030)(WINDTM(J,I),J=13,24)
455 CONTINUE
DO 460 I=1,90
WRITE(6,4040)(CURRTM(J,I),J=1,8)
WRITE(6,4040)(CURRTM(J,I),J=9,16)
WRITE(6,4040)(CURRTM(J,I),J=17,24)
460 CONTINUE
4030 FORMAT(1X,12I6)
4040 FORMAT(1X,8I8)
WRITE(6,4050)
4050 FORMAT(1H0,* WIND SEQUENCE ONE *//)
WRITE(6,4060)(IWNDSEQ(1,J),J=1,30)
WRITE(6,4060)(IWNDSEQ(1,J),J=31,60)
WRITE(6,4060)(IWNDSEQ(1,J),J=61,90)
4060 FORMAT(1X,30I2)
WRITE(6,4070)
4070 FORMAT(1H0,* WIND SEQUENCE TWO *//)
WRITE(6,4060)(IWNDSEQ(2,J),J=1,30)
WRITE(6,4060)(IWNDSEQ(2,J),J=31,60)

GOTO 500
490 WRITE(6,5000)

```

```

5000 FORMAT(1H0,*START 'DAY IS BEFORE DATA *')
500 STOP
END

```

```

REAL FUNCTION AVMAG(ILO,IDA)
INTEGER WINDTM
DIMENSION U(12),V(12)
COMMON/WNDATA/WINDTM(24,90)
DATA U,V/12*0.0,12*0.0/
DATA XNSAM/12.0/
IF(ILO.EQ.2)GOTO 20
DO 15 I = 1,6
    IF(WINDTM(IDA-1,I+18).LT.0)XNSAM = XNSAM-1
    IF(WINDTM(IDA-1,I+18).LT.0)GOTO 11
    CALL CNVWND(WINDTM(IDA-1,I+18),U(I),V(I))
11    IF(WINDTM(IDA,I).LT.0)XNSAM = XNSAM-1
    IF(WINDTM(IDA,I).LT.0)GOTO 15
    CALL CNVWND(WINDTM(IDA,I),U(I+6),V(I+6))
15 CONTINUE
    GOTO 50
20 DO 25 I = 1,12
    IF(WINDTM(IDA,I+6).LT.0)XNSAM = XNSAM-1
    IF(WINDTM(IDA,I+6).LT.0)GOTO 25
    CALL CNVWND(WINDTM(IDA,I+6),U(I),V(I))
25 CONTINUE
50 AVMAG = 0.0
    DO 60 I = 1,12
        AVMAG = AVMAG + SQRT((U(I)**2)+(V(I)**2))/XNSAM
60 CONTINUE
RETURN
END

```

```

SUBROUTINE CNVWND(IVEL,UW,VW)
VSUR = FLOAT(IVEL-1000*IFIX(.001*FLOAT(IVEL)))
USUR = (FLOAT(IVEL)-VSUR)*.001
UW = USUR*.1 - 50.0
VW = VSUR*.1 - 50.0
RETURN
END

```

```

SUBROUTINE CNVCUR(ICUR,UC,VC)
VSUR = FLOAT(ICUR-10000*IFIX(.0001*FLOAT(ICUR)))
USUR = (FLOAT(ICUR)-VSUR)*.0001
UC = (USUR-5000)*0.1
VC = (VSUR-5000)*0.1
C THIS RECREATES CURRENT IN ITS ORIGINAL UNITS WHICH WAS
C CM/SEC. NOW CONVERT TO M/SEC FOR USE BY PROGRAM.
UC = UC*1.0E-2
VC = VC*1.0E-2
RETURN
END

```